Characteristics and sources of submicron aerosols above the urban canopy (260 m) in Beijing, China during 2014 APEC summit

C. Chen[1,2,3], Y. L. Sun[1,2*], W. Q. Xu[1], W. Du[1,3], L. B. Zhou[1], T. T. Han[1], Q. Q. Wang[1], P. Q. Fu[1], Z. F. Wang[1], Z. Q. Gao[1,2], Q. Zhang[4], D. R. Worsnop[5]

[1]*State Key Laboratory of Atmospheric Boundary Layer Physics and Atmospheric Chemistry, Institute of Atmospheric Physics, Chinese Academy of Sciences, Beijing China*

[2] *Collaborative Innovation Center on Forecast and Evaluation of Meteorological Disasters, Nanjing University of Information Science & Technology, Nanjing, China*

[3]*College of Applied Meteorology, Nanjing University of Information Science and Technology, Nanjing, China*

[3]*Department of Resources and Environment, Air Environmental Modeling and Pollution Controlling Key Laboratory of Sichuan Higher Education Institutes, Chengdu University of Information Technology, Chengdu, China*

[4]*Department of Environmental Toxicology, University of California, 1 Shields Ave., Davis, CA 95616, USA*

[5]*Aerodyne Research, Inc., Billerica, MA, USA*

*Correspondence to Y. L. Sun (sunyele@mail.iap.ac.cn)

Abstract

The megacity of Beijing has experienced frequent severe fine particle pollution during the last decade. Although the sources and formation mechanisms of aerosol particles have been extensively investigated on the basis of ground measurements, real-time characterization of aerosol particle composition and sources above the urban canopy in Beijing is rare. In this study, we conducted real-time measurements of non-refractory submicron aerosol (NR-PM_1) composition at 260 m at the 325 m Beijing Meteorological Tower (BMT) from October 10 to November 12, 2014, by using an aerosol chemical speciation monitor (ACSM) along with synchronous measurements of size-resolved NR-PM_1 composition at near ground level using a High-Resolution Time-of-Flight Aerosol Mass Spectrometer (HR–ToF–AMS). The NR-PM_1 composition above the urban canopy was dominated by organics (46%), followed by nitrate (27%) and sulfate (13%). The high contribution of nitrate and high NO_3^-/SO_4^{2-} mass ratios illustrate an important role of nitrate in particulate matter (PM) pollution during the study period. The organic aerosol (OA) was mainly composed by secondary OA (SOA), accounting for 61% on an average. Different from that measured at the ground site, primary OA (POA) correlated moderately with SOA, likely suggesting a high contribution from regional transport above the urban canopy. The Asia–Pacific Economic Cooperation (APEC) summit with strict emission controls provides a unique opportunity to study the impacts of emission controls on aerosol chemistry. All aerosol species were shown to have significant decreases of 40–80% during APEC from those measured before APEC, suggesting that emission controls over regional scales substantially reduced PM levels. However, the bulk aerosol composition was relatively similar before and during APEC as a result of synergetic controls of aerosol precursors. In addition to emission controls, the routine circulations of mountain–valley breezes were also found to play an important role in alleviating PM levels and achieving the "APEC blue" effect. The evolution of vertical differences between 260 m and the ground level was also investigated. Our results show complex vertical differences during the formation and evolution of severe haze episodes that are closely related to aerosol sources and boundary layer dynamics.

1 Introduction

Beijing (39°56′N, 116°20′ E), the capital of China, is one of the largest megacities in the world with more than 21 million residents and 5.4 million vehicles in operation by the end of 2013 (Beijing Municipal Bureau of Statistics, 2014). In the west, north, and northeast, the city is surrounded by the Taihang and Yanshan mountains at approximately 1000–1500 m above sea level. The fan-shaped topography in addition to the rapid urbanization has caused frequent severe haze pollution episodes in Beijing. These conditions have received a significant amount of attention from atmospheric scientists, the government, and the general public (Sun et al., 2006;Sun et al., 2012a;Sun et al., 2013c;Guo et al., 2014;Sun et al., 2014). For in-depth elucidation of severe urban haze formation and particulate matter (PM) characteristics, extensive studies have been conducted in Beijing including real-time online measurements and filter sampling with subsequent offline analyses (Sun et al., 2006;Pope III et al., 2009;Zhao et al., 2013). Aerosol Mass Spectrometers (AMS), which are capable of determining size-resolved aerosol compositions with high sensitivity, have been widely deployed in Beijing and other cities in China since 2006 (Huang et al., 2012b;Zhang et al., 2014;Li et al., 2015). Numerous conclusions and findings have been obtained since then, which have greatly improved our understanding of aerosol composition, formation mechanisms, and evolution processes (Sun et al., 2010;Xiao et al., 2011;Zhang et al., 2012;Hu et al., 2013;Huang et al., 2013;Guo et al., 2014;Zhang et al., 2014;Li et al., 2015). However, most previous AMS studies include short-term measurements, of generally less than two months, because of the high cost and maintenance of the instrument. The recently developed aerodyne aerosol chemical speciation Monitor (ACSM) (Ng et al., 2011) has been used in some studies for examining the chemical composition, sources, and processes of atmospheric aerosols in China. The advantage of the ACSM is its robustness for real-time long-term measurements of aerosol particle composition with little attendance (Ng et al., 2011;Sun et al., 2012a;Sun et al., 2013c;Budisulistiorini et al., 2014;Sun et al., 2014;Parworth et al., 2015;Petit et al., 2015). The first ACSM measurements in Beijing highlighted the important role of nitrate in PM pollution in summer, which

was mainly attributed to the partitioning of nitric acid into liquid ammonium nitrate particles (Sun et al., 2012a). The PM pollution characteristics also dramatically differed between summer and winter. Agricultural burning and photochemical production play major roles in PM pollution in summer (Li et al., 2010;Huang et al., 2012a;Sun et al., 2012a;Zhang et al., 2015), whereas coal combustion is the dominant source of PM in winter (Sun et al., 2013c). A more detailed analysis of a severe haze pollution episode occurred in January 2013 suggested that stagnant meteorological conditions, source emissions, secondary production and regional transport are four major factors driving the formation and evolution of haze pollution in Beijing during winter (Sun et al., 2013c;Guo et al., 2014;Sun et al., 2014;Zhang et al., 2014).

Despite extensive efforts for the characterization of fine particle pollution in Beijing, most studies are conducted at ground sites, which are subject to significant influences of local emission sources such as traffic, cooking, and biomass burning. In comparison, measurements obtained above the urban canopy with much less influence of local source are more representative for a large scale, which is of great importance for characterizing regional transport. However, such studies in Beijing are rare due to the absence of high platforms. The 325 m Beijing Meteorological Tower (BMT) is a unique platform for measuring aerosol and gaseous species at various heights in Beijing megacity. Moreover, this platform is beneficial for studying the interactions of the lower boundary layer (<300 m) and air pollution, particularly during autumn and winter when the nocturnal planetary boundary height is often below 300 m (Ting et al., 2008;Zhang et al., 2013). Based on the BMT measurements, Sun et al. (2009;2013a) reported that the SO_2 concentration reached its maximal value at 50 m during heating periods, whereas $PM_{2.5}$ showed a “higher top and lower bottom” vertical pattern due to the inversions of temperature (*T*) and relative humidity (RH) during summer hazy days. Guinot et al. (2006) and Meng et al. (2008) also determined that local concentration peaks at 50 m to 100 m were likely related to the urban canopy. However, real-time characterization of aerosol particle composition above the urban canopy has been performed only once (Sun et al., 2015). The two-week study found substantially different aerosol compositions between ground level and 260 m. In

addition, the compositional differences at the two heights were found to be strongly associated with source emissions, the vertical mixing mechanism, and RH/*T*-dependent secondary production. Because these measurements only lasted two weeks, the aerosol characteristics and sources above the urban canopy remain poorly understood.

The 2014 Asia–Pacific Economic Cooperation (APEC) summit was hosted in Beijing during November 5–11, 2014, when strict emission control measures were implemented in Beijing and surrounding regions to ensure the air quality. During November 3–12, emission controls such as reducing the number of vehicles in operation by approximately 50%, shutting down factories, stopping construction activities, and enhancing the cleanliness of urban roads were gradually implemented (http://www.bjepb.gov.cn/bjepb/323474/331443/331937/333896/412827/index.html, in Chinese). The neighboring provinces such as Hebei, Tianjin, and Shandong implemented the same emission controls during APEC (http://www.bjepb.gov.cn/bjepb/324122/412670/index.html, in Chinese). As a result, the PM levels in Beijing during the summit were significantly reduced, leading to "APEC blue," a phrase commonly used to refer to the good air quality. However, the response of aerosol chemistry to emission controls over a regional scale has not been investigated. Measurements above the urban canopy are ideal for evaluating the roles of emission controls in reducing PM levels under the condition of minimizing the influences of local point sources.

In this study, we conduct real-time measurements of non-refractory submicron aerosol (NR-PM_1) composition including organics (Org), sulfate (SO_4^{2-}), nitrate (NO_3^-), ammonium (NH_4^+), and chloride (Cl^-) at 260 m at the BMT before and during APEC, October 10–November 2 and November 3–12, 2014, respectively, by using an ACSM. The aerosol composition, diurnal variation, and sources above the urban canopy are investigated in detail. The responses of aerosol composition, particle acidity, and sources of organic aerosol (OA) to emission controls are elucidated by comparing the changes before and during APEC, and the roles of meteorological conditions in PM reduction during APEC are discussed. In addition, the vertical

differences of aerosol composition and its interactions with boundary layer dynamics are also examined.

2 Experimental methods

2.1 Sampling site and measurements

All of the measurements in this study were conducted at the same site as that reported by Sun et al. (2013c), which is an urban site at the Institute of Atmospheric Physics, Chinese Academy of Sciences, between North 3rd and 4th Ring Road from October 10 to 12 November, 2014. The ACSM and gas measurement instruments were mounted inside a container at 260 m on the BMT. The ACSM sampling setup used in this study is similar to that described by Sun et al. (2012a). Briefly, aerosol particles were first sampled into the container with a $PM_{2.5}$ cyclone to remove coarse particles larger than 2.5 μm. After passing through a diffusion silica-gel dryer, aerosol particles were sampled into the ACSM at a flow rate of ~0.1 L/min. The ACSM was operated by alternating ambient air and filtered air with a mass spectrometer at a scanning rate of 500 ms amu^{-1} from *m/z* 10 to 150. The data were saved every two cycles, leading to a time resolution of approximately 5 min. The detailed principles of the ACSM can be found elsewhere (Ng et al., 2011;Sun et al., 2012a). An Aerodyne High-Resolution Time-of-Flight AMS (HR-ToF-AMS) was simultaneously deployed near the ground level at the same location to measure the size-resolved NR-PM_1 aerosol composition. Details of the sampling and operation procedures of the HR-ToF-AMS was given in Xu et al. (2015).

Meteorological variables including wind speed (WS), wind direction (WD), RH, and *T* at 15 heights of 8, 15, 32, 47, 65, 100, 120, 140, 160, 180, 200, 280, and 320 m were obtained from the BMT. In addition, a Doppler wind lidar (Windcube 200, Leosphere, Orsay, France) was deployed at the same location to obtain the wind profiles from 100 m to 5000 m with a spatial resolution of 50 m and a time resolution of 10 min. All of the data in this study are reported in Beijing Standard Time (BST), which equals Coordinated Universal Time (UTC) plus 8 h.

2.2 Data analysis

The ACSM data were analyzed for the mass concentration and chemical composition of NR-PM_1 species including organics, sulfate, nitrate, ammonium, and chloride by using ACSM standard data analysis software (v. 1.5.3.0). Detailed analytical procedures have been reported by Ng et.al (2011) and Sun et.al (2012a). Similar to that in previous studies in Beijing (Sun et al., 2011;Sun et al., 2012a;Sun et al., 2013c;Sun et al., 2014), an empirical and constant collection efficiency (CE) of 0.5 was applied during the entire campaign to compensate for the particle loss due mainly to particle bounce at the vaporizer (Matthew et al., 2008). The CE of 0.5 is rationale for this study because aerosol particles were dried, and the mass fraction of ammonium nitrate was overall below the threshold value (40%) that affects CE (Middlebrook et al., 2012). The average ratio of measured NH_4^+ ($NH_4^+{}_{meas}$) versus predicted NH_4^+ ($NH_4^+{}_{pred}$) was 0.56, suggesting that the aerosol particles were acidic. Although the particle acidity would have a slightly higher CE than 0.5 (~0.59) if the equation $CE_{dry} = \max(0.45, 1.0 - 0.73 \times (NH_4^+{}_{meas}/NH_4^+{}_{pred}))$ recommended by Middlebrook et al. (2012) were used, no effect on CE is present if using the parameterization reported by Quinn et al. (2006). For consistency with our previous studies and with the HR-ToF-AMS measurements at the ground site, we maintained CE = 0.5 in this study. The default relative ionization efficiency (RIE) values, 1.4 for organics, 1.1 for nitrate, 1.2 for sulfate, and 1.3 for chloride except ammonium (6.5) which was determined from pure ammonium nitrate particles. Note that the ACSM measurements were compared with those of HR-AMS at the same location before the campaign. All submicron aerosol species measured by the ACSM were highly correlated with those by the HR-AMS ($r^2 > 0.97$). Although the total NR-PM_1 mass measured by the ACSM agreed well with that by HR-AMS ($r^2 = 0.99$, slope = 0.99), the regression slopes of ACSM against HR-AMS varied from 0.61–1.24 for different aerosol species. Because ACSM was found to have a larger uncertainty in quantification of submicron aerosol species, particularly in determination of relative ionization efficiency, the mass concentrations of aerosol species measured by the ACSM at 260 m were further corrected using the regression slopes of ACSM/HR-AMS obtained from the inter-comparison study.

Positive matrix factorization (PMF) with the PMF2.exe algorithm (Paatero and Tapper, 1994) was performed on the ACSM OA mass spectra to resolve potential OA components with different sources and processes. Only *m/z*'s < 125 was included in the PMF analysis due to the large interferences of naphthalene signals on several larger *m/z*'s (e.g., *m/z* 127–129) (Sun et al., 2012a;Sun et al., 2013c;Sun et al., 2014). The PMF results were then evaluated by using an Igor Pro-based PMF Evaluation Tool (PET, v 2.06) (Ulbrich et al., 2009) with following procedures detailed by Zhang et al. (2011). After careful evaluation of the mass spectra and time series of OA factors, a two-factor solution, i.e., an oxygenated OA (OOA) and a hydrocarbon-like OA (HOA) with fpeak = 0.4, was chosen. A more detailed PMF diagnostics is presented in Figs. S1, S2 and Table S1. While the 3-factor solution resolved an unrealistic factor with unexpectedly high *m/z* 12 and *m/z* 15, the 2-factor solution at fpeak = 0 showed much higher *m/z* 44 in HOA spectrum, which is generally a characteristics of OOA (Fig. S3).

2.3 Air mass trajectory analyses

The three-day (72 h) back trajectories were calculated every hour at 500 m height using the Hybrid Single-Particle Lagrangian Integrated Trajectory (HYSPLIT, NOAA) 4.9 model (Draxler and Hess, 1997;Li et al., 2015). The trajectories were then grouped into four clusters before and during APEC using the algorithm of cluster analysis. The clustering of trajectories is based on the total spatial variance (TSV) method (Draxler et al., 2012). This method minimizes the inter-cluster differences among trajectories while maximizing the inter-cluster differences, which has been widely used in previous studies (Sun et al., 2014;Zhang et al., 2014;Li et al., 2015)

3 Results and discussion

3.1 General description

3.1.1 Submicron aerosol and meteorology

The NR-PM_1 mass concentration varied significantly from 0.7 to 254 μg m^{-3}, with an average of 53.5 μg m^{-3}. As indicated in Fig. 1, the variations of NR-PM_1 were strongly associated with WD and WS. The formation of severe haze episodes was generally initiated by a WD change from northerly to southerly and a decrease of WS

to less than 5 m s^{-1} below 1 km. The southern air flow and low WS were then dominant most of the time during the evolution of haze episode; subsequently, the air masses changed from the south to the north/northwest, leading to a rapid decrease of PM level in a few hours. Haze episodes with such life cycle driven by meteorological conditions have also been observed many times in Beijing (Jia et al., 2008;Sun et al., 2013c;Guo et al., 2014;Sun et al., 2014). Note that a mountain–valley breeze lasting approximately half a day was frequently observed throughout the study, which reduced the daytime PM levels to a certain degree. As shown in Fig. 1, most of the cleaning processes were similar, all driven by the switch of air masses from south/southwest to north/northwest associated with high WS across the entire vertical layer (>5 m s^{-1}). However, the cleaning process occurring on October 20–21 was different. As the WD changed from the south to the northwest/northeast, the NR-PM_1 concentration remained high. This phenomenon can be explained by the low WS (<4 m s^{-1}) below 500 m and the high RH (Figs. 2, S4). The NR-PM_1 began to decrease at ~20:00 as WD shifted to the south associated with a decrease in RH. This result indicates that a cleaner and dryer air mass was located to the south of Beijing during this stage. Such a cleaning process by southern air flow is not common and is generally weaker than that by northern/northwestern flow. This observation is supported by the higher NR-PM_1 concentration of ~20 μg m^{-3} on October 21 than during other cleaning periods at ~<5 μg m^{-3}. The average mass concentration of NR-PM_1 during APEC was 24.1 μg m^{-3}, which is significantly lower than the 65.1 μg m^{-3} recorded before APEC, indicating a large reduction of PM during APEC. In addition, the southern air mass occurred less frequently and had a shorter duration during APEC. These results manifest that meteorology in addition to emission controls might have played an important role in reducing PM levels during APEC.

The NR-PM_1 species showed similar and dramatic variations to the total NR-PM_1 mass (Fig. 2). In particular, three haze episodes before APEC (Ep1, Ep2, and Ep3 in Fig. 2d) and two episodes during the summit (APEC1 and APEC2 in Fig. 2d) were observed in this study. The three episodes before APEC were all characterized by high RH at 48–70% and low WS at 2.3–3.4 m s^{-1}, elucidating the important roles of

stagnant meteorological conditions in severe haze formation. In comparison, the RH in the two episodes during APEC was lower at 34–38%, and the WS was comparably higher at 3.1–3.8 m s^{-1} (Table 1). These results suggest that the meteorological conditions during APEC appeared to be more favorable for dispersion of pollutants. Indeed, clear accumulation processes of aerosol species were observed for three episodes before APEC, yet they were much weaker during the summit. However, the two episodes during APEC showed obvious temperature inversions, which inhibited the vertical convection of pollutants. The meteorological conditions during haze episodes differed substantially from those during clean periods, which were characterized by high WS at >5 m s^{-1} and low RH at <20%.

The NR-PM_1 was dominated by organics, accounting for on average 46% of the total mass, followed by nitrate at 27%, sulfate at 13%, ammonium at 9%, and chloride at 5%. The nitrate contribution ranged from 27% to 28% during the three episodes before APEC and from 29% to 31% in the two episodes during APEC, which is significantly higher than the sulfate contribution of 10–15% and 8–11%, respectively (Fig. 6). Although the dominance of organics in PM_1 was consistent with that in previous studies in Beijing (Sun et al., 2012a;Sun et al., 2013c;Guo et al., 2014;Sun et al., 2014;Zhang et al., 2014), the nitrate contribution in this study was approximately twice that of sulfate and significantly higher than previously reported values of 16% in 2011 (Sun et al., 2013c) and 13–14% in 2013 (Sun et al., 2014;Zhang et al., 2014). The mass ratio of NO_3^-/SO_4^{2-}can be used to indicate the relative importance of mobile and stationary sources (Arimoto et al., 1996). Therefore, higher NO_3^-/SO_4^{2-} in this study likely indicates the predominance of mobile source rather than stationary source. Because the continuous increase of NO_x emissions associated with a decrease in SO_2 (Wang et al., 2013), nitrate is expected to play a more important role in PM pollution in the future. Our results highlight that NO_x emission control should be a priority in mitigating air pollution, particularly in non-heating seasons with low SO_2 precursors.

Figure 3 further shows the time series of NO_3^-/SO_4^{2-}mass ratio and sulfur oxidation ratio (SOR) calculated as the molar fraction of sulfate in total sulfur (i.e.,

sulfate and SO_2) (Sun et al., 2014). The NO_3^-/SO_4^{2-} was ubiquitously greater than 1 during five haze episodes, indicating the importance of nitrate in the formation of severe haze pollution. Interestingly, we observed a rapid increase in NO_3^-/SO_4^{2-} during the formation stage of a pollution episode followed by a decrease in NO_3^-/SO_4^{2-} during the subsequent evolution stage. The variations of NO_3^-/SO_4^{2-} illustrate that two different formation mechanisms might drive the formation and evolution of haze episodes. During the early stage of haze formation, the RH was relatively low and the formation rate of sulfate was correspondingly low, which is supported by the low SOR values. Consequently, the nitrate formation played a dominant role during this stage. The SO_4^{2-} concentration remained consistently low when the nitrate began to increase (Fig. 2d). As the RH continued to increase, the SOR showed a corresponding increase indicating that more SO_2 was oxidized to form sulfate, most likely via aqueous-phase processing (Zhang and Tie, 2011;Sun et al., 2013b). The SO_4^{2-} concentration then showed a substantial increase, and the NO_3^-/SO_4^{2-} ratio decreased as a result. For example, during Ep2, the hourly NO_3^-/SO_4^{2-} increased from ~1.1 to 4.0 during the formation stage and then decreased to ~1.8 during the evolution stage. These results indicate that SO_4^{2-} played an enhanced role in PM pollution during the evolution stage of haze episodes with high RH. Moreover, the NO_3^-/SO_4^{2-} ratios during clean periods (~0.3) were much lower than those during haze episodes. One explanation is that the nitrate in clean air masses from north/northwest is significantly lower than that of sulfate.

3.1.2 Sources and composition of OA

Two OA factors, HOA and OOA, were identified in this study. The HOA spectrum was similar to those determined at other urban sites (Huang et al., 2012a;Sun et al., 2012a;Sun et al., 2012b), which is characterized by prominent hydrocarbon ion peaks of *m/z* 27, 29, 41, 43, 55, 57 (Fig. 4a). The HOA spectrum showed a higher *m/z* 55/57 ratio compared with that of exhaust aerosols from diesel trucks and gasoline vehicles (Mohr et al., 2009), yet it had characteristics similar to those resolved in urban Beijing (Sun et al., 2010;Sun et al., 2012a). The high *m/z* 55/57 ratio and the two visible peaks at meal times in diurnal variations (Fig. 4b)

indicate the impact of local cooking activities (Sun et al., 2011;Sun et al., 2012a;Sun et al., 2013c). However, the two HOA peaks were much smaller than those observed at the ground site (Xu et al., in preparation), indicating a significantly smaller impact of local cooking emissions on OA at 260 m. Moreover, the HOA spectrum showed a considerable *m/z* 60 peak, a marker *m/z* for biomass burning (Aiken et al., 2009;Huang et al., 2011;Zhang et al., 2015). The fraction of *m/z* 60 was 0.9%, which is much higher than ~0. 3% in the absence of biomass burning. All these results suggest that HOA was a primary OA factor combined with traffic, cooking, and biomass burning emissions. Limited by the ACSM spectra and PMF analysis, we were not able to separate the different primary OA factors in this study. HOA correlated well with chloride ($r^2 = 0.61$) and moderately well with secondary inorganic species ($r^2 = 0.42–0.65$), indicating that a major fraction of HOA shared similar sources to secondary species at 260 m, which was likely from regional transport. HOA on average contributed 39% of total organics, which is less than the 57% observed at the ground site during the same study period (Xu et al., in preparation). This result indicates a smaller impact of primary sources above the urban canopy. The diurnal cycle of HOA was relatively flat with two visible peaks occurring at noon and night. The HOA contribution to OA was relatively constant throughout the day, ranging from 36% to 43%. This result further supports the theory that HOA above the urban canopy was dominantly from regional transport and was well mixed with regional secondary OA (SOA). Indeed, the correlation of HOA with OOA in this study was quite high ($r^2 = 0.76$), supporting that HOA and OOA might have some common sources (e.g., regional transport) at 260 m.

The mass spectrum of OOA resembles that identified in 2012 in summer in Beijing (Sun et al., 2012a) in addition to those resolved at other urban sites (Ulbrich et al., 2009), which is characterized by a prominent *m/z* 44 peak (mainly CO_2^+). OOA dominated the OA composition throughout the day, ranging from 57% to 64%. The average OOA contribution to OA was 61%, which is close to those previously reported in Beijing (Huang et al., 2010;Sun et al., 2012a;Sun et al., 2013c). The diurnal cycle of OOA was relatively flat, yet a gradual increase during the day was

also observed despite the rising planetary boundary layer, suggesting daytime photochemical processing. OOA is often considered as a good surrogate of SOA (Zhang et al., 2005;Jimenez et al., 2009;Ng et al., 2011). In this study, OOA tracked well with secondary inorganic species such as NO_3^-, SO_4^{2-} (r^2 = 0.72–0.90), which is consistent with previous conclusions that OOA is a secondary species in nature (Zhang et al., 2005;Sun et al., 2012a).

3.2 Response of aerosol chemistry to emission controls

3.2.1 Aerosol composition

Figure 5 shows the variations of aerosol composition as a function of NR-PM_1 mass loading before and during APEC. The organics contribution showed a notable decrease from 62% to 32% as the NR-PM_1 mass concentration increased from <10 μg m^{-3} to >200 μg m^{-3} before APEC. In contrast, the sulfate contribution showed a corresponding increase from 8% to 22%. Except for low values at NR-PM_1 <10 μg m^{-3}, nitrate and ammonium constituted relatively constant fractions of NR-PM_1 across different NR-PM_1 loadings and varied at 21–31% and 8–12%, respectively. These results highlighted the enhanced roles of secondary inorganic species in severe PM pollution before APEC. This observation is further supported by a comparison of average chemical composition between three pollution episodes and a clean event (Fig. 6). The secondary inorganic aerosol (SIA = SO_4^{2-} + NO_3^- + NH_4^+) on average contributed 46–51% of the total NR-PM_1 mass during the three episodes before APEC, which is significantly higher than the 40% reported during the clean event (Fig. 6). The NR-PM_1 mass loading-dependent aerosol composition showed a different behavior during APEC. As shown in Fig. 5b, all aerosol species had relatively constant contributions to NR-PM_1 at 10–100 μg m^{-3}. The contribution of organics ranged from 43% to 58%, which is overall higher than those before APEC. This result indicates an enhanced role of organics during APEC, particularly during severe PM pollution periods. Similarly, nitrate contributed the largest fraction of NR-PM_1, varying from 23% to 32%. Figure 5 also shows a very broad range of NR-PM_1 mass concentration with the maximum concentration over 200 μg m^{-3} before APEC. In contrast, the range of NR-PM_1 was much narrower during APEC, suggesting a

significantly lower amount of severe haze pollution during APEC. Indeed, 93% of the time during APEC, the NR-PM_1 level was lower than 60 μg m^{-3}, whereas 49% of the time before APEC exceeded such a concentration level. These results indicate that the air pollution was substantially more severe before APEC. The average mass concentration of NR-PM_1 was 24.1 μg m^{-3} during APEC, which is 63% lower than the 65.1 μg m^{-3} recorded before APEC (Fig. 6). This result demonstrates a significant reduction of PM during APEC due to emission controls and better weather conditions including higher WS and lower RH. However, the bulk NR-PM_1 composition was rather similar before and during APEC, both of which were dominated by organics, 46% versus 47%, followed by nitrate at 27% versus 29% and sulfate at 14% versus 10% (Fig. 6). The lower sulfate contribution during APEC might due to the lower RH, leading to less production of sulfate. These results highlight that the emission controls during APEC did not significantly affect the regional aerosol bulk composition, although the mass concentrations of precursors and aerosol species were reduced substantially. One possible explanation is the synergetic control of various precursors such as SO_2, NO_x, and volatile organic compounds (VOCs) over a regional scale during APEC. Our results clearly imply that synergetic controls of the emissions of precursors over a regional scale are efficient for mitigating air pollution in North China.

3.2.2 Diurnal variations

The diurnal variations of meteorological variables, NR-PM_1 species, and OA components before and during APEC are presented in Fig. 7. The diurnal cycles of meteorological conditions were overall similar before and during APEC except for lower temperatures and RH during APEC. The WS during APEC was consistently higher than that before APEC, particularly in the morning (04:00–12:00) and evening (18:00–22:00). Although the WD during APEC was dominantly from the northwest at night and shifted to the south during the day, it was mainly from the south before APEC (Fig. 2c).

The total NR-PM_1 showed pronounced diurnal variation with two peaks in early afternoon (12:00–14:00) and late evening (20:00–22:00) that were dominantly

412 influenced by organics. By checking the diurnal cycles of the OA factors, we
413 concluded that the two peaks occurring at meal times are mainly attributed to primary
414 emissions such as cooking-related activities and traffic emissions (Allan et al.,
415 2010;Sun et al., 2011;Sun et al., 2012a). Compared with the diurnal cycles of OA
416 previously observed at the ground site in Beijing (Sun et al., 2012a), the two peaks of
417 organics were considerably smaller. This result indicates that local source emissions
418 can be vertically mixed above the urban canopy but at substantially reduced
419 concentrations. Our results also demonstrate that sampling above the urban canopy is
420 less influenced by local source emissions and can be more representative over a
421 regional scale.

422 SIA and OOA showed similar diurnal patterns before and during APEC, all of
423 which were characterized by gradual increases during the day. These results indicate
424 that their diurnal cycles were driven by similar formation mechanisms before and
425 during APEC such as photochemical processing and daytime vertical mixing. Higher
426 concentrations of secondary species were also observed at night, which might have
427 been associated with a shallower boundary layer height (Sun et al., 2012a). It should
428 be noted that all secondary species showed relatively constant background
429 concentrations, indicating that a major fraction was likely from regional transport. SIA
430 and OOA during APEC showed substantial reductions (45–74%) throughout the day
431 compared with those before APEC, indicating that regional emission controls played a
432 significant role in reducing secondary species during APEC, although the lower RH
433 and higher WS were also important. Moreover, a higher reduction percentage was
434 observed between 04:00 and 12:00, when higher mountain–valley breezes occurring
435 routinely during APEC cleaned the air pollutants more efficiently.

436 The diurnal cycles of chloride showed some differences before and during APEC.
437 Although it was relatively flat during APEC, chloride showed a clear decrease in the
438 afternoon before APEC, likely due to the evaporative loss and dilution effects
439 associated with higher *T* and the elevated boundary layer (Sun et al., 2012a). The
440 diurnal cycle of HOA showed overall lower concentration during the day except for a
441 pronounced noon peak before and during APEC. Considering that the peak time

corresponds to lunch time, we concluded that it was attributed mainly to local cooking sources. In addition, a more significant reduction in evening peak of HOA was observed during APEC. One explanation is that controls of heavy-duty vehicles (HDV) and heavy-duty diesel trucks (HDDT) decreased the HOA emissions at night during APEC.

3.2.3 Particle acidity

Particle acidity is a key parameter that influences aerosol toxicity, hygroscopic growth, and heterogeneous reactions (Sun et al., 2010). In this study, we evaluated aerosol particle acidity by using the ratio of measured NH_4^+ ($NH_4^+_{meas}$) to predicted NH_4^+ ($NH_4^+_{pred}$), which requires full neutralization of SO_4^{2-}, NO_3^-, and Cl^-: $NH_4^+_{pred} = 18 \times (2 \times SO_4^{2-}/96 + NO_3^-/62 + Cl^-/35.5)$ (Zhang et al., 2007a). Lower $NH_4^+_{meas}/NH_4^+_{pred}$ indicates greater aerosol particle acidity. As shown in Fig. 8, $NH_4^+_{meas}$ strongly correlated with $NH_4^+_{pred}$ before and during APEC (r^2 = 0.95 and 0.91, respectively), with regression slopes of 0.56 and 0.62, respectively. Slopes less than 1 indicate that aerosol particles above the urban canopy were acidic both before and during APEC. It should be noted that we might overestimate the particle acidity by counting all chloride as NH_4Cl. As indicated by the prominent *m/z* 60 in HOA spectrum, biomass burning could be an important source of primary aerosol at 260 m. Considering that chloride from biomass burning emissions could exist in the form of KCl, the approach recommended by Zhang et al. (2007a) would overestimate the predicted NH_4^+ and hence the aerosol particle acidity. Compared with the ground site measurement, $NH_4^+_{meas}/NH_4^+_{pred}$ = 0.75 and 0.80 for the periods before and during APEC, respectively, aerosol particles were more acidic above the urban canopy. One reason is that the concentration of SO_2 was higher above the urban canopy than that at the ground site (Meng et al., 2008). Another possible explanation is that the NH_3 from traffic emissions (Li et al., 2006;Meng et al., 2011) can neutralize more secondary inorganic aerosol near the ground level. Moreover, we detected a slight decrease in particle acidity during APEC, which is consistent with the slightly higher reduction of sulfate than other inorganic species. One reason is likely the slightly greater reduction of SO_2 than other gaseous precursors during APEC. It is also possible that the lower

RH during APEC decreased the aqueous-phase formation of sulfate and hence decreased particle acidity. Overall, the slight change in aerosol particle acidity revealed that the joint emission controls appear to have not affected the particle acidity significantly over regional scales, which is consistent with the small changes in aerosol composition before and during APEC.

3.2.4 Meteorological effects

Meteorological parameters contribute the largest uncertainties in evaluating the effects of emission controls on PM reduction. Here we compared the variations of aerosol species as a function of RH and WS before and during APEC. At low RH levels (<40%), all aerosol species appeared to increase linearly as a function of RH in both periods at similar rates of increase. Moreover, the mass concentrations of aerosol species were slightly lower during APEC than those before the summit, indicating small reductions in aerosol species during APEC. By checking the air mass trajectories (Fig. S5), we determined that the low RH periods were mainly associated with the air masses from the north/northwest where fewer emission controls were implemented during APEC. This finding explains the small reductions in aerosol species (~22%) during APEC under the same RH conditions. However, the variations in aerosol species showed substantially different behaviors as a function of RH at high RH levels (>40%) before and during APEC. Whereas most aerosol species continued to linearly increase as function of RH before APEC, they remained relatively constant and even showed deceases during APEC. As a result, significant reductions in aerosol species at high RH levels were observed during APEC. The air masses during high RH periods were found to be dominantly from the south/southeast where strict emission controls were implemented such as Hebei, Tianjin, and Shandong provinces. These results clearly indicate that emission controls played a major role in PM reduction during APEC and that the control effects tended to be more efficient under higher RH periods. The primary HOA and chloride showed decreases when the RH was >60%, indicating that humidity has a significantly lower impact on primary aerosols than secondary components at high RH levels.

The mass concentrations of aerosol species showed a strong dependence on WS

before and during APEC. For example, the total NR-PM_1 mass was decreased by ~80% from ~100 μg m^{-3} to < 20 μg m^{-3} as WS increased to 7 m s^{-1} before APEC. These results indicate that wind is efficient in cleaning air pollutants in Beijing, which is consistent with previous conclusions (Han et al., 2009;Sun et al., 2013c). In comparison, the decreasing rates of aerosol species as a function of WS were lower during APEC. As a result, aerosol species showed the largest concentration differences before and during APEC in periods with low WS. As indicated by the wind increase plots in Fig. 10, low and high WS were mainly associated with southern/southeastern and northern/northwestern winds, respectively. These results further indicate that larger reductions of aerosol species occurred in Beijing when air masses were from the south.

3.2.5 Back trajectory analysis

Figure 11 presents the average chemical composition of NR-PM_1, corresponding to four clusters before and during APEC, determined from the cluster analysis of back trajectories (Draxler and Hess, 1997). The air masses before APEC were predominantly from the south/southeast at 54% of the time (C1 in Fig. 11a), and the aerosol loading was the highest (96.7 μg m^{-3}) among the clusters. Comparatively, the northwesterly clusters (C3 and C4 in Fig. 11a) presented significantly lower aerosol loadings at 8.3 μg m^{-3} and 3.5 μg m^{-3}, respectively, with fewer frequencies of 14% and 11%, respectively. Such large differences in aerosol loadings between the northerly and southerly air masses are consistent with the spatial distributions of anthropogenic emissions such as SO_2, NO_x, and BC (Zhang et al., 2007b;Lu et al., 2011). Although the areas to the north/northwest of Beijing are relatively clean with low emissions of anthropogenic primary pollutants, the south/southeast regions are characterized by substantially higher emissions. In addition, 21% of the air masses originated from the west and showed moderately high NR-PM_1 mass at 55.4 μg m^{-3}. It should be noted that the air masses from the south were often stagnant, as indicated by their shorter trajectories, which played an important role in facilitating the accumulation of pollutants. The aerosol composition varied significantly among four clusters, reflecting the variety in chemical characteristics of aerosol particles from

different source regions. The aerosol particle composition from the southeastern and western clusters (C1 and C2) were dominated by nitrate at 27% and 30% and OOA at 26% and 32%, respectively, with considerable contribution from sulfate at 14% and 10%, respectively. These results elucidate the dominant roles of nitrate and OOA in severe PM pollution before APEC, which differs significantly from previous studies reporting that sulfate was generally more prevalent than nitrate (Huang et al., 2014;Sun et al., 2014). These results also highlight a very different pollution characteristic during the late fall season from that in winter. In comparison, the nitrate contributions were significantly lower, at 17% and 8%, in the two northwestern clusters (C3 and C4) associated with an enhanced contribution of sulfate at 19% and 21%, respectively. Moreover, the cleanest cluster (C4) showed a dominant contribution of organics at 64%, indicating the important role of organics during clean periods (Sun et al., 2010;Sun et al., 2013c).

The air masses during APEC showed changes, particularly the increases in frequency of two northwestern clusters (C1 and C4), which was 40% of the time compared with 25% before APEC (Fig. 11b). These two clusters showed similar bulk aerosol compositions to those before APEC yet with reductions of the total NR-PM_1 mass loading at nearly 40–50%. The air masses during APEC were dominated by cluster 3 (C3 in Fig. 11b). Although C3 originated from the north of Beijing, it circulated around the south of Beijing including Baoding, a polluted city in Hebei province, before arriving at the sampling site. As a result, C3 presented the highest aerosol mass loading, at 44.0 μg m^{-3}, composed primarily of nitrate and OOA at 30% and 29%, respectively. Moreover, cluster 2 (C2 in Fig. 11b), originating from the northwest, showed a similar aerosol composition yet had an ~50% decrease in total mass compared to C3. One explanation is that air masses in C2 passed through the western Beijing, where is relatively cleaner than the southeastern regions. As shown in Fig. 11, similar clusters before and during APEC showed ubiquitous reductions in NR-PM_1 mass during APEC, indicating that emission controls played an important role in PM reduction. Moreover, the decreases in frequency of southern/southeastern air masses during APEC also helped to alleviate the PM level for the entire period,

thus achieving the "APEC blue" effect. Emission controls in surrounding regions south of Beijing should be taken as a priority for mitigation of air pollution in Beijing.

3.3 Vertical differences: insights into emission controls and boundary layer dynamics

Figure 12 shows a comparison of the time series of NR-PM_1 species between 260 m and the ground level for the entire study. All submicron species showed overall similar variations at the two different heights, indicating their relatively similar sources and evolution processes. However, large vertical differences in aerosol composition were also frequently observed, illustrating complex vertical gradients of aerosol species caused by multiple factors such as local emissions, regional transport, and boundary layer dynamics. The average compositional differences before and during APEC are shown in Fig. 13. Although the concentration difference in NR-PM_1 was close before and during APEC at 12.1 μg m^{-3} and 14.1 μg m^{-3}, respectively, the composition differed significantly. SIA dominated the compositional difference before APEC, together accounting for 95% of the total NR-PM_1 mass. In comparison, organics and chloride showed minor vertical differences (<5%). These results indicate different sources and formation mechanisms between SIA and organic aerosol. During APEC, the compositional difference was dominated by organics, accounting for 68% on average, and the contributions of SIA were largely reduced at 25%. These results suggest that emission controls over regional scales affect the composition differences between ground level and the urban canopy. As discussed in section 3.2 and by Xu et al. (2015), secondary species including SIA and SOA showed significant reductions at both ground level and 260 m during APEC as a result of emission controls. Although primary OA showed similar reductions as those of SOA above the urban canopy, the changes remained small near the ground level. Thus, the largest organic difference during APEC was mainly caused by local primary source emissions.

The vertical differences in aerosol composition also varied largely among different haze episodes. As indicated in Fig. 12 and Table 1, Ep3 presented the smallest vertical differences for all aerosol species, indicating a well-mixed layer below 260 m. The WS was consistently low at <2.5 m s^{-1} across the different heights,

592 and the WD was predominantly from the south during Ep3. Moreover, the vertical
593 profiles of extinction showed an evident reduction in pollution from ~2 km to the
594 ground on October 28, leading to the formation of Ep3 (Fig. S6). Such boundary layer
595 dynamics would produce a well-mixed layer in the lower atmosphere, leading to
596 minor chemical differences between the ground level and 260 m.

597 Comparatively, the vertical evolution of Ep2 differed significantly (Fig. 14a). The
598 mass concentrations of all aerosol species between the ground level and 260 m were
599 similar during the formation stage of Ep2, from October 23 to 9:00 October 24.
600 However, although aerosol species near the ground level showed large increases after
601 9:00 on October24, they remained relatively constant at 260 m, leading to the largest
602 vertical concentration gradients among five episodes. The average NR-PM_1 at 260 m
603 was 143.4 μg m^{-3}, which is 38% lower than that at the ground site. By checking the
604 vertical profiles of meteorological variables, we observed a clear temperature
605 inversion between 120 m and 160 m that formed during 0:00–9:00 on October 24.
606 Such a temperature inversion formed a stable layer below ~200 m and inhibited the
607 vertical mixing of air pollutants between the ground and 260 m. In addition, the
608 stagnant meteorological conditions as indicated by low WS and high RH further
609 facilitated the accumulation of ground pollution. It should be noted that the
610 aqueous-phase processing, most likely fog processing under the high RH conditions
611 (often > 90%) during this stage, also played an important role in the increase of SIA,
612 particularly sulfate. This finding is also supported by the significant increase of SOR
613 during this stage (Fig. 3).

614 The evolution of the severe Ep2 was terminated at approximately 0:00 on October
615 26 when the WD changed from south to northwest. Although the mass concentrations
616 of aerosol species at 260 m began to show rapid decreases at that time, the
617 concentration at the ground site decreased significantly after 4 hours. The different
618 cleaning processes between 260 m and the ground level are closely linked to the
619 vertical profiles of meteorological variables. As indicated in Fig. 14a, a strong
620 temperature inversion below 320 m was observed during the cleaning period, which
621 resulted in a significantly higher WS and lower RH at 260 m than those at ground

622 level. Indeed, both WS and RH showed clear shears during the cleaning period,
623 suggesting a gradual interaction between the northern air mass and boundary pollution
624 from top to bottom. Such an interacting mechanism resulted in a time lag of
625 approximately 4 h in cleaning the pollutants at ground level over that at 260 m.
626 Similar interactions between boundary layer dynamics and aerosol pollution were also
627 observed on November 1, 5, and 11.

628 The evolution of vertical differences during APEC differed from those in three
629 episodes before APEC. As shown in Fig. 14b, frequent mountain–valley breezes were
630 observed during November 8–11 (APEC2). The northwest mountain–valley breeze
631 began routinely at approximately midnight and dissipated at approximately noon. The
632 NR-PM_1 aerosol species showed direct responses to the mountain–valley breeze,
633 which was characterized by similar routine diurnal cycles. All aerosol species began
634 to decrease at midnight because the cleaning effects of mountain–valley breeze
635 reached minimum concentrations at noon, then increased continuously when the WD
636 changed to south. The mountain–valley breeze also caused a unique diurnal cycle of
637 vertical differences. As shown in Fig. 14b, aerosol species were well mixed within the
638 lower boundary layer between 12:00 and 16:00, and the concentrations between 260
639 m and the ground level were similar. However, the differences in concentration began
640 to increase when the boundary layer height decreased after sunset at ~18:00, and the
641 differences were maximum at midnight when the NR-PM_1 mass approached 100 μg
642 m^{-3}. A detailed check of the evolution of aerosol species showed that such vertical
643 differences in NR-PM_1 were caused mainly by organics from local primary sources
644 (Xu et al. in preparation; Fig. 12). These results indicate that local source emissions
645 played a more important role in PM pollution near ground level during APEC. The
646 concentration differences in NR-PM_1 began to decrease with the occurrence of the
647 mountain–valley breeze and reached a minimum at noon. Our results revealed the
648 important role of mountain–valley breeze in affecting the boundary layer structure and
649 reducing the daytime PM levels during APEC. It was estimated that the
650 mountain–valley breeze caused a reduction in NR-PM_1 concentration of
651 approximately 50 μg m^{-3} at the ground site during the day on November 10–11 (Fig.

14b). Therefore, our results illustrated that the achievement of "APEC blue" was also due partly to meteorological effects, particularly the mountain–valley breeze, in addition to emission controls.

4 Conclusions

We have presented a detailed characterization of aerosol particle composition and sources above the urban canopy in Beijing from October 10 to November 12, 2014. This study is unique because it examines strict emission controls implemented during the 2014 APEC summit and synchronous real-time measurements of aerosol particle composition at 260 m and that near the ground level obtained by two aerosol mass spectrometers. The NR-PM_1 composition above the urban canopy was dominated by organics at 46%, followed by nitrate at 27% and sulfate at 13%. The high contribution of nitrate and high NO_3^-/SO_4^{2-} mass ratios illustrate the important role of nitrate in PM pollution during the study period. This result has significant implications that NO_x emission controls should be prioritized for the mitigation of air pollution in Beijing, particularly in non-heating seasons with low SO_2 precursors. The OA above the urban canopy was dominated by OOA at 61% and included HOA at 39%. Different from that at the ground site, HOA correlated moderately with OOA above the urban canopy, indicating similar sources likely through regional transport.

With the implementation of emission controls, the mass concentrations of aerosol species were shown to have decreased significantly by 40–80% during APEC, whereas the bulk aerosol composition was relatively similar before and during APEC. Organics were dominant before and during the summit, at 46% versus 47%, respectively, followed by nitrate at 27% versus 29% and sulfate at 14% versus 10%, respectively. Our results suggest that synergetic controls of various precursors such as SO_2, NO_x, and VOCs over a regional scale would not significantly affect regional aerosol bulk composition, although the mass concentrations would be reduced substantially. By linking aerosol compositions and sources to meteorological conditions, we determined that meteorological parameters, particularly mountain–valley breezes, played an important role in suppressing PM growth and hence reducing PM levels during APEC. Our results elucidated that the good air

quality in Beijing during APEC was the combined result of emission controls and meteorological effects, with the former playing the dominant role. We further investigated the vertical evolution of aerosol particle composition by comparing the aerosol chemistry between the ground level and 260 m. We observed very complex vertical differences during the formation and evolution of severe haze episodes that were closely related to aerosol sources (local versus regional) and boundary layer dynamics. Although a stable *T* inversion layer between 120 m and 160 m associated with stagnant meteorology caused higher concentrations of aerosol species at the ground site, the interaction of boundary layer dynamics and aerosol chemistry during the cleaning processes resulted in a lag time of approximately 4 h in cleaning pollutants near the ground level over those occurring above the urban canopy.

Acknowledgements

This work was supported by the National Key Project of Basic Research (2014CB447900), the Strategic Priority Research Program (B) of the Chinese Academy of Sciences (XDB05020501), the Key Research Program of the Chinese Academy of Sciences (KJZD-EW-TZ-G06-01-0), and the Special Fund for Environmental Protection Research in the Public Interest (201409001).

References

Aiken, A. C., Salcedo, D., Cubison, M. J., Huffman, J. A., DeCarlo, P. F., Ulbrich, I. M., Docherty, K. S., Sueper, D., Kimmel, J. R., Worsnop, D. R., Trimborn, A., Northway, M., Stone, E. A., Schauer, J. J., Volkamer, R. M., Fortner, E., de Foy, B., Wang, J., Laskin, A., Shutthanandan, V., Zheng, J., Zhang, R., Gaffney, J., Marley, N. A., Paredes-Miranda, G., Arnott, W. P., Molina, L. T., Sosa, G., and Jimenez, J. L.: Mexico City aerosol analysis during MILAGRO using high resolution aerosol mass spectrometry at the urban supersite (T0) - Part 1: Fine particle composition and organic source apportionment, Atmos. Chem. Phys., 9, 6633-6653, 2009.

Allan, J., Williams, P., Morgan, W., Martin, C., Flynn, M., Lee, J., Nemitz, E., Phillips, G., Gallagher, M., and Coe, H.: Contributions from transport, solid fuel burning and cooking to primary organic aerosols in two UK cities, Atmos. Chem. Phys., 10, 647-668, 2010.

Arimoto, R., Duce, R., Savoie, D., Prospero, J., Talbot, R., Cullen, J., Tomza, U., Lewis, N., and Ray, B.: Relationships among aerosol constituents from Asia and the North Pacific during PEM‐West A, Journal of Geophysical Research: Atmospheres (1984–2012), 101, 2011-2023, 1996.

Budisulistiorini, S., Canagaratna, M., Croteau, P., Baumann, K., Edgerton, E., Kollman, M., Ng, N., Verma, V., Shaw, S., and Knipping, E.: Intercomparison of an Aerosol Chemical Speciation Monitor (ACSM) with ambient fine aerosol measurements in downtown Atlanta, Georgia, Atmospheric Measurement Techniques, 7, 1929-1941, 2014.

Draxler, R. R., and Hess, G.: Description of the HYSPLIT4 modeling system, Air Resources Laboratory, Silver Spring, Maryland, 1997.

Guinot, B., Roger, J.-C., Cachier, H., Pucai, W., Jianhui, B., and Tong, Y.: Impact of vertical atmospheric structure on Beijing aerosol distribution, Atmos. Environ., 40, 5167-5180, 2006.

Guo, S., Hu, M., Zamora, M. L., Peng, J., Shang, D., Zheng, J., Du, Z., Wu, Z., Shao, M., and Zeng, L.: Elucidating severe urban haze formation in China, Proc. Natl. Acad. Sci. U.S.A., 111, 17373-17378, 2014.

Han, S., Kondo, Y., Oshima, N., Takegawa, N., Miyazaki, Y., Hu, M., Lin, P., Deng, Z., Zhao, Y., and Sugimoto, N.: Temporal variations of elemental carbon in Beijing, Journal of Geophysical Research: Atmospheres (1984–2012), 114, D23202, doi:23210.21029/22009JD012027, 2009.

Hu, W. W., Hu, M., Yuan, B., Jimenez, J. L., Tang, Q., Peng, J., Hu, W., Shao, M., Wang, M., and Zeng, L.: Insights on organic aerosol aging and the influence of coal combustion at a regional receptor site of central eastern China, Atmos. Chem. Phys, 13, 095, 2013.

Huang, K., Zhuang, G., Lin, Y., Fu, J., Wang, Q., Liu, T., Zhang, R., Jiang, Y., Deng, C., and Fu, Q.: Typical types and formation mechanisms of haze in an Eastern Asia megacity, Shanghai, Atmos. Chem. Phys., 12, 105-124, 2012a.

Huang, R. J., Zhang, Y., Bozzetti, C., Ho, K. F., Cao, J. J., Han, Y., Daellenbach, K. R., Slowik, J. G., Platt, S. M., Canonaco, F., Zotter, P., Wolf, R., Pieber, S. M., Bruns,

744 E. A., Crippa, M., Ciarelli, G., Piazzalunga, A., Schwikowski, M., Abbaszade, G.,
745 Schnelle-Kreis, J., Zimmermann, R., An, Z., Szidat, S., Baltensperger, U., El
746 Haddad, I., and Prevot, A. S.: High secondary aerosol contribution to particulate
747 pollution during haze events in China, Nature, 514, 218-222,
748 10.1038/nature13774, 2014.
749 Huang, X.-F., He, L.-Y., Hu, M., Canagaratna, M., Sun, Y., Zhang, Q., Zhu, T., Xue,
750 L., Zeng, L.-W., and Liu, X.-G.: Highly time-resolved chemical characterization
751 of atmospheric submicron particles during 2008 Beijing Olympic Games using an
752 Aerodyne High-Resolution Aerosol Mass Spectrometer, Atmos. Chem. Phys., 10,
753 8933-8945, 2010.
754 Huang, X.-F., He, L.-Y., Xue, L., Sun, T.-L., Zeng, L.-W., Gong, Z.-H., Hu, M., and
755 Zhu, T.: Highly time-resolved chemical characterization of atmospheric fine
756 particles during 2010 Shanghai World Expo, Atmos. Chem. Phys., 12, 4897-4907,
757 2012b.
758 Huang, X.-F., Xue, L., Tian, X.-D., Shao, W.-W., Sun, T.-L., Gong, Z.-H., Ju, W.-W.,
759 Jiang, B., Hu, M., and He, L.-Y.: Highly time-resolved carbonaceous aerosol
760 characterization in Yangtze River Delta of China: Composition, mixing state and
761 secondary formation, Atmos. Environ., 64, 200-207, 2013.
762 Huang, X. F., He, L. Y., Hu, M., Canagaratna, M. R., Kroll, J. H., Ng, N. L., Zhang, Y.
763 H., Lin, Y., Xue, L., Sun, T. L., Liu, X. G., Shao, M., Jayne, J. T., and Worsnop, D.
764 R.: Characterization of submicron aerosols at a rural site in Pearl River Delta of
765 China using an Aerodyne High-Resolution Aerosol Mass Spectrometer, Atmos.
766 Chem. Phys., 11, 1865-1877, 10.5194/acp-11-1865-2011, 2011.
767 Jia, Y., Rahn, K. A., He, K., Wen, T., and Wang, Y.: A novel technique for quantifying
768 the regional component of urban aerosol solely from its sawtooth cycles, J.
769 Geophys. Res., 113, D21309, 10.1029/2008jd010389, 2008.
770 Jimenez, J., Canagaratna, M., Donahue, N., Prevot, A., Zhang, Q., Kroll, J., DeCarlo,
771 P., Allan, J., Coe, H., and Ng, N.: Evolution of organic aerosols in the atmosphere,
772 Science, 326, 1525-1529, 2009.
773 Li, W., Shao, L., and Buseck, P.: Haze types in Beijing and the influence of
774 agricultural biomass burning, Atmos. Chem. Phys., 10, 8119-8130, 2010.
775 Li, Y., Schwab, J. J., and Demerjian, K. L.: Measurements of ambient ammonia using
776 a tunable diode laser absorption spectrometer: Characteristics of ambient
777 ammonia emissions in an urban area of New York City, J. Geophys. Res., 111,
778 D10S02, 10.1029/2005jd006275, 2006.
779 Li, Y., Lee, B., Su, L., Fung, J., and Chan, C.: Seasonal characteristics of fine
780 particulate matter (PM) based on high-resolution time-of-flight aerosol mass
781 spectrometric (HR-ToF-AMS) measurements at the HKUST Supersite in Hong
782 Kong, Atmos. Chem. Phys., 15, 37-53, 2015.
783 Lu, Z., Zhang, Q., and Streets, D. G.: Sulfur dioxide and primary carbonaceous
784 aerosol emissions in China and India, 1996–2010, Atmos. Chem. Phys., 11,
785 9839-9864, 10.5194/acp-11-9839-2011, 2011.
786 Matthew, B. M., Middlebrook, A. M., and Onasch, T. B.: Collection efficiencies in an
787 Aerodyne Aerosol Mass Spectrometer as a function of particle phase for

laboratory generated aerosols, Aerosol Sci. Tech., 42, 884-898, 2008.
Meng, Z., Ding, G., Xu, X., Xu, X., Yu, H., and Wang, S.: Vertical distributions of SO 2 and NO 2 in the lower atmosphere in Beijing urban areas, China, Sci. Total Environ., 390, 456-465, 2008.
Meng, Z., Lin, W., Jiang, X., Yan, P., Wang, Y., Zhang, Y., Jia, X., and Yu, X.: Characteristics of atmospheric ammonia over Beijing, China, Atmos. Chem. Phys., 11, 6139-6151, 2011.
Middlebrook, A. M., Bahreini, R., Jimenez, J. L., and Canagaratna, M. R.: Evaluation of composition-dependent collection efficiencies for the aerodyne aerosol mass spectrometer using field data, Aerosol Sci. Tech., 46, 258-271, 2012.
Mohr, C., Huffman, J. A., Cubison, M. J., Aiken, A. C., Docherty, K. S., Kimmel, J. R., Ulbrich, I. M., Hannigan, M., and Jimenez, J. L.: Characterization of primary organic aerosol emissions from meat cooking, trash burning, and motor vehicles with high-resolution aerosol mass spectrometry and comparison with ambient and chamber observations, Environ. Sci. Technol., 43, 2443-2449, 2009.
Ng, N. L., Herndon, S. C., Trimborn, A., Canagaratna, M. R., Croteau, P., Onasch, T. B., Sueper, D., Worsnop, D. R., Zhang, Q., and Sun, Y.: An Aerosol Chemical Speciation Monitor (ACSM) for routine monitoring of the composition and mass concentrations of ambient aerosol, Aerosol Sci. Tech., 45, 780-794, 2011.
Paatero, P., and Tapper, U.: Positive matrix factorization: A non‐negative factor model with optimal utilization of error estimates of data values, Environmetrics, 5, 111-126, 1994.
Parworth, C., Fast, J., Mei, F., Shippert, T., Sivaraman, C., Tilp, A., Watson, T., and Zhang, Q.: Long-term measurements of submicrometer aerosol chemistry at the Southern Great Plains (SGP) using an Aerosol Chemical Speciation Monitor (ACSM), Atmos. Environ., 106, 43-55, 2015.
Petit, J.-E., Favez, O., Sciare, J., Crenn, V., Sarda-Estève, R., Bonnaire, N., Močnik, G., Dupont, J.-C., Haeffelin, M., and Leoz-Garziandia, E.: Two years of near real-time chemical composition of submicron aerosols in the region of Paris using an Aerosol Chemical Speciation Monitor (ACSM) and a multi-wavelength Aethalometer, Atmos. Chem. Phys., 15, 2985-3005, 2015.
Pope III, C. A., Ezzati, M., and Dockery, D. W.: Fine-particulate air pollution and life expectancy in the United States, New England Journal of Medicine, 360, 376-386, 2009.
Quinn, P., Bates, T., Coffman, D., Onasch, T., Worsnop, D., Baynard, T., De Gouw, J., Goldan, P., Kuster, W., and Williams, E.: Impacts of sources and aging on submicrometer aerosol properties in the marine boundary layer across the Gulf of Maine, J. Geophys. Res.: Atmos. (1984–2012), 111, D23S36, doi:10.1029/2006jd007582, 2006.
Sun, J., Zhang, Q., Canagaratna, M. R., Zhang, Y., Ng, N. L., Sun, Y., Jayne, J. T., Zhang, X., Zhang, X., and Worsnop, D. R.: Highly time-and size-resolved characterization of submicron aerosol particles in Beijing using an Aerodyne Aerosol Mass Spectrometer, Atmos. Environ., 44, 131-140, 2010.
Sun, Y.-L., Zhang, Q., Schwab, J., Demerjian, K., Chen, W.-N., Bae, M.-S., Hung,

H.-M., Hogrefe, O., Frank, B., and Rattigan, O.: Characterization of the sources and processes of organic and inorganic aerosols in New York city with a high-resolution time-of-flight aerosol mass apectrometer, Atmos. Chem. Phys., 11, 1581-1602, 2011.

Sun, Y., Zhuang, G., Tang, A., Wang, Y., and An, Z.: Chemical characteristics of PM2. 5 and PM10 in haze-fog episodes in Beijing, Environ. Sci. Technol., 40, 3148-3155, 2006.

Sun, Y., Wang, Y., and Zhang, C.: Measurement of the vertical profile of atmospheric SO 2 during the heating period in Beijing on days of high air pollution, Atmos. Environ., 43, 468-472, 2009.

Sun, Y., Wang, Z., Dong, H., Yang, T., Li, J., Pan, X., Chen, P., and Jayne, J. T.: Characterization of summer organic and inorganic aerosols in Beijing, China with an Aerosol Chemical Speciation Monitor, Atmos. Environ., 51, 250-259, 2012a.

Sun, Y., Zhang, Q., Schwab, J., Yang, T., Ng, N., and Demerjian, K.: Factor analysis of combined organic and inorganic aerosol mass spectra from high resolution aerosol mass spectrometer measurements, Atmos. Chem. Phys., 12, 8537-8551, 2012b.

Sun, Y., Song, T., Tang, G., and Wang, Y.: The vertical distribution of PM 2.5 and boundary-layer structure during summer haze in Beijing, Atmos. Environ., 74, 413-421, 2013a.

Sun, Y., Wang, Z., Fu, P., Jiang, Q., Yang, T., Li, J., and Ge, X.: The impact of relative humidity on aerosol composition and evolution processes during wintertime in Beijing, China, Atmos. Environ., 77, 927-934, 2013b.

Sun, Y., Wang, Z., Fu, P., Yang, T., Jiang, Q., Dong, H., Li, J., and Jia, J.: Aerosol composition, sources and processes during wintertime in Beijing, China, Atmos. Chem. Phys., 13, 4577-4592, 2013c.

Sun, Y. L., Jiang, Q., Wang, Z., Fu, P., Li, J., Yang, T., and Yin, Y.: Investigation of the sources and evolution processes of severe haze pollution in Beijing in January 2013, J. Geophys. Res.: Atmos., 119, 4380-4398, 2014.

Sun, Y., Du, W., Wang, Q., Zhang, Q., Chen, C., Chen, Y., Chen, Z., Fu, P., Wang, Z., Gao, Z., and Worsnop, D.: Real-Time Characterization of Aerosol Particle Composition above the Urban Canopy in Beijing: Insights into the Interactions between the Atmospheric Boundary Layer and Aerosol Chemistry, Environ. Sci. Technol., 49, 11340–11347, 10.1021/acs.est.5b02373, 2015.

Ting, M., Yue-Si, W., Jie, J., Fang-Kun, W., and Mingxing, W.: The vertical distributions of VOCs in the atmosphere of Beijing in autumn, Sci. Total Environ., 390, 97-108, 2008.

Ulbrich, I., Canagaratna, M., Zhang, Q., Worsnop, D., and Jimenez, J.: Interpretation of organic components from Positive Matrix Factorization of aerosol mass spectrometric data, Atmos. Chem. Phys., 9, 2891-2918, 2009.

Wang, Y., Zhang, Q. Q., He, K., Zhang, Q., and Chai, L.: Sulfate-nitrate-ammonium aerosols over China: response to 2000–2015 emission changes of sulfur dioxide, nitrogen oxides, and ammonia, Atmos. Chem. Phys., 13, 2635-2652, 10.5194/acp-13-2635-2013, 2013.

Xiao, R., Takegawa, N., Zheng, M., Kondo, Y., Miyazaki, Y., Miyakawa, T., Hu, M., Shao, M., Zeng, L., and Gong, Y.: Characterization and source apportionment of submicron aerosol with aerosol mass spectrometer during the PRIDE-PRD 2006 campaign, Atmos. Chem. Phys., 11, 6911-6929, 2011.

Xu, W., Sun, Y., Chen, C., Du, W., Han, T., Wang, Q., Fu, P., Wang, Z., Zhao, X., and Zhou, L.: Aerosol composition, oxidative properties, and sources in Beijing: results from the 2014 Asia-Pacific Economic Cooperation Summit study, Atmospheric Chemistry and Physics Discussions, 15, 23407-23455, 2015.

Zhang, J., Sun, Y., Liu, Z., Ji, D., Hu, B., Liu, Q., and Wang, Y.: Characterization of submicron aerosols during a month of serious pollution in Beijing, 2013, Atmos. Chem. Phys., 14, 2887-2903, 2014.

Zhang, Q., Worsnop, D., Canagaratna, M., and Jimenez, J.: Hydrocarbon-like and oxygenated organic aerosols in Pittsburgh: insights into sources and processes of organic aerosols, Atmos. Chem. Phys., 5, 3289-3311, 2005.

Zhang, Q., Jimenez, J. L., Worsnop, D. R., and Canagaratna, M.: A case study of urban particle acidity and its effect on secondary organic aerosol, Environ. Sci. Technol., 41, 3213-3219, 2007a.

Zhang, Q., Streets, D. G., He, K., Wang, Y., Richter, A., Burrows, J. P., Uno, I., Jang, C. J., Chen, D., Yao, Z., and Lei, Y.: NOx emission trends for China, 1995-2004: The view from the ground and the view from space, J. Geophys. Res., 112, D22306, 10.1029/2007jd008684, 2007b.

Zhang, Q., Jimenez, J. L., Canagaratna, M. R., Ulbrich, I. M., Ng, N. L., Worsnop, D. R., and Sun, Y.: Understanding atmospheric organic aerosols via factor analysis of aerosol mass spectrometry: a review, Anal. Bioanal. Chem., 401, 3045-3067, 2011.

Zhang, Q., and Tie, X.: High solubility of SO2: evidence in an intensive fog event measured in the NCP region, China, Atmos. Chem. Phys. Discuss., 11, 2931-2947, 10.5194/acpd-11-2931-2011, 2011.

Zhang, Q., Meng, J., Quan, J., Gao, Y., Zhao, D., Chen, P., and He, H.: Impact of aerosol composition on cloud condensation nuclei activity, Atmos. Chem. Phys., 12, 3783-3790, 2012.

Zhang, W., Zhang, Y., Lv, Y., Li, K., and Li, Z.: Observation of atmospheric boundary layer height by ground-based LiDAR during haze days, Journal of Remote Sensing, 17, 981-992, 2013.

Zhang, Y., Tang, L., Wang, Z., Yu, H., Sun, Y., Liu, D., Qin, W., Canonaco, F., Prévôt, A., and Zhang, H.: Insights into characteristics, sources, and evolution of submicron aerosols during harvest seasons in the Yangtze River delta region, China, Atmos. Chem. Phys., 15, 1331-1349, 2015.

Zhao, X., Zhao, P., Xu, J., Meng, W., Pu, W., Dong, F., He, D., and Shi, Q.: Analysis of a winter regional haze event and its formation mechanism in the North China Plain, Atmos. Chem. Phys., 13, 5685-5696, 2013.

Table 1. Summary of average meteorological variables for different periods and the mass differences of aerosol species between ground site and 260 m (= ground – 260 m).

	Before APEC				During APEC		
	Entire	Ep1	Ep2	Ep3	Entire	APEC1	APEC2
Meteorological Variables							
RH (%)	47.1	48.4	69.7	56.7	29.8	34.2	38.5
T (°C)	13.3	16.7	12.5	10.9	9.0	11.5	8.1
WS (m s^{-1})	4.0	3.4	2.3	2.3	4.9	3.8	3.1
Mass Differences (μg m^{-3})							
Org	0.7	0.3	4.5	-5.2	9.6	14.6	13.6
SO_4^{2-}	3.4	3.0	8.8	1.3	1.3	1.6	1.9
NO_3^-	4.3	4.5	10.9	0.8	0.7	1.0	1.0
NH_4^+	3.9	4.2	9.0	2.3	1.6	2.9	2.3
Cl^-	-0.1	0.0	-0.4	-0.2	1.0	1.7	1.5
NR-PM_1	12.1	12.0	32.8	-1.1	14.1	21.8	20.2

Figure captions:

Figure 1. Evolution of vertical profiles of (a) wind speed (WS) and (b) wind direction (WD) from the measurements of the Doppler wind lidar.The time series of NR-PM_1 (=Org + SO_4^{2-} + NO_3^- + NH_4^+ + Cl^-) is shown as the black line in (a). The shaded area refers to the APEC period (same for following figures).

Figure 2. Time series of (a) *T*, (b) RH, (c) WS and WD, (d) NR-PM_1 species (Org, SO_4^{2-}, NO_3^-, NH_4^+, and Cl^-), and (f) mass fraction of each species in NR-PM_1. Two clean periods and five haze episodes are marked in Fig. 2d for further discussions. The meteorological parameters in this figure were all from the tower measurements.

Figure 3. Time series of (a) sulfur oxidation ratio (SOR), (b) ratio of NO_3^-/SO_4^{2-}, and (c) NR-PM_1. The SOR and NO_3^-/SO_4^{2-} were color coded by RH.

Figure 4. (a) Mass spectra of HOA and OOA, (b) diurnal variations of the mass concentration and mass fraction of HOA and OOA, (c) time series of HOA, OOA, and inorganic species (SO_4^{2-}, NO_3^-, Cl^-). The correlations of HOA and OOA with inorganic specie are also shown in the figure.

Figure 5. Submicron aerosol composition as a function of NR-PM_1 mass loadings (a) before APEC and (b) during APEC. The solide line shows the probability of NR-PM_1 mass.

Figure 6. Average chemical composition of NR-PM_1 before and during APEC, and also that of five haze episodes and two clean events marked in Fig. 2.

Figure 7. Diurnal variations of meteorological variables (*T*, RH, WS, and WD), NR-PM_1 species, and OA factors before and during APEC. The change rates during APEC (= (Before APEC –APEC)/ Before APEC × 100) are also marked as light gray in the figure.

Figure 8. Correlations between measured NH_4^+ and predicted NH_4^+ (= 18× (2×SO_4^{2-}/96 + NO_3^-/62 + Cl^-/35.5)) before and during APEC. The inset plot shows the correlations of measured NH_4^+ vs. predicted NH_4^+ at the ground site.

Figure 9. Variations of NR-PM_1 species and OA factors as a function of (a) RH and (b) WS before and during APEC. The RH and WS were from the tower measurements at 280 m.

Figure 10. Wind rose plots (a) before APEC and (b) during APEC.

Figure 11. The average NR-PM_1 composition for each cluster (a) before and (b) during APEC. The numbers on the pie charts refer to the average total NR-PM_1 mass for each cluster. In addition, the number of trajectories and its percentage to the total trajectories are also shown in the legends.

Figure 12. Comparisons of time series of total NR-PM_1 mass and NR-PM_1 species between 260 m and ground level.

Figure 13. Average chemical composition of the difference between ground level and 260 m (a) before APEC and (b) during APEC. The "1%" in the box indicates lower concentration of chloride at ground site than 260 m.

Figure 14. The evolution of vertical profiles of meteorological variables (WD, WS, RH, and *T*), and NR-PM_1 concentration at 260 m and ground site during two pollution episodes (a) Ep2 and (b) APEC2. The vertical profiles of wind speed and wind

direction were from the measurements of the Doppler wind lidar, and those of RH and *T* were from the tower measurements. The white areas in the figure indicate that the data were not available.

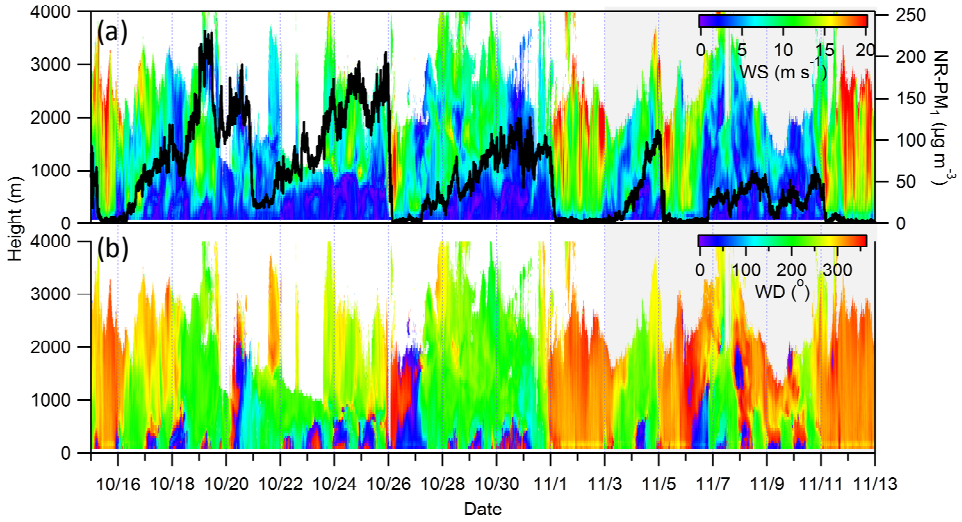

969

970 **Figure 1.** Evolution of vertical profiles of (a) wind speed (WS) and (b) wind direction
971 (WD) from the measurements of the Doppler wind lidar. The time series of NR-PM_1
972 (= Org + SO_4^{2-} + NO_3^- + NH_4^+ + Cl^-) is shown as the black line in (a). The shaded
973 area refers to the Asia–Pacific Economic Cooperation (APEC) summit period, which
974 is the same in the following figures.

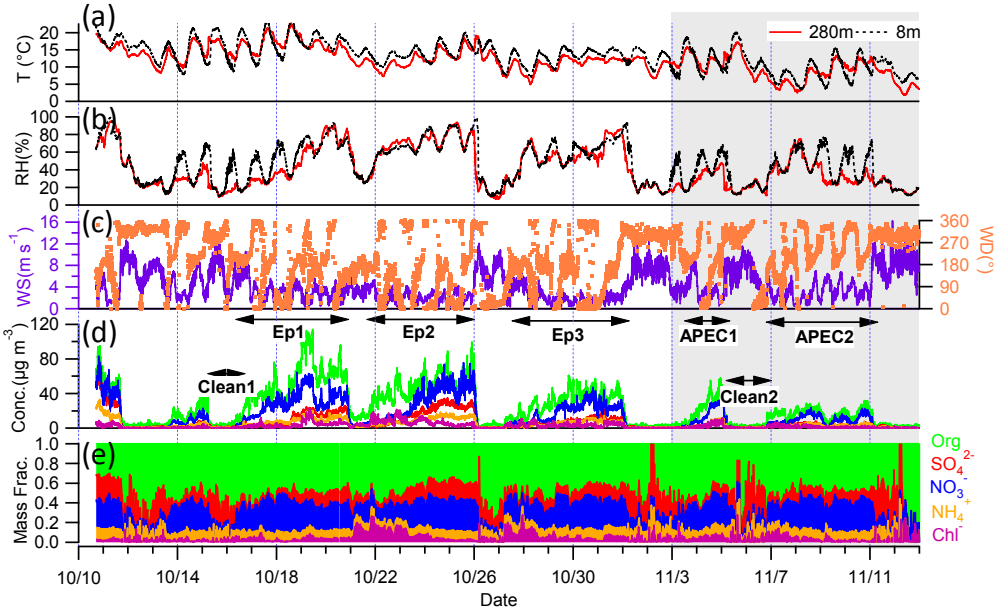

975

976 **Figure 2.** Time series of (a) temperature (*T*), (b) relative humidity (RH), (c) wind
977 speed (WS) and wind direction (WD), (d) non-refractory submicron aerosol (NR-PM_1)
978 species (Org, SO_4^{2-}, NO_3^-, NH_4^+, and Cl^-), and (f) mass fraction of each species in
979 NR-PM_1. Two clean periods and five haze episodes are marked in Fig. 2d for further
980 discussion. The meteorological parameters in this figure were all from the tower
981 measurements.

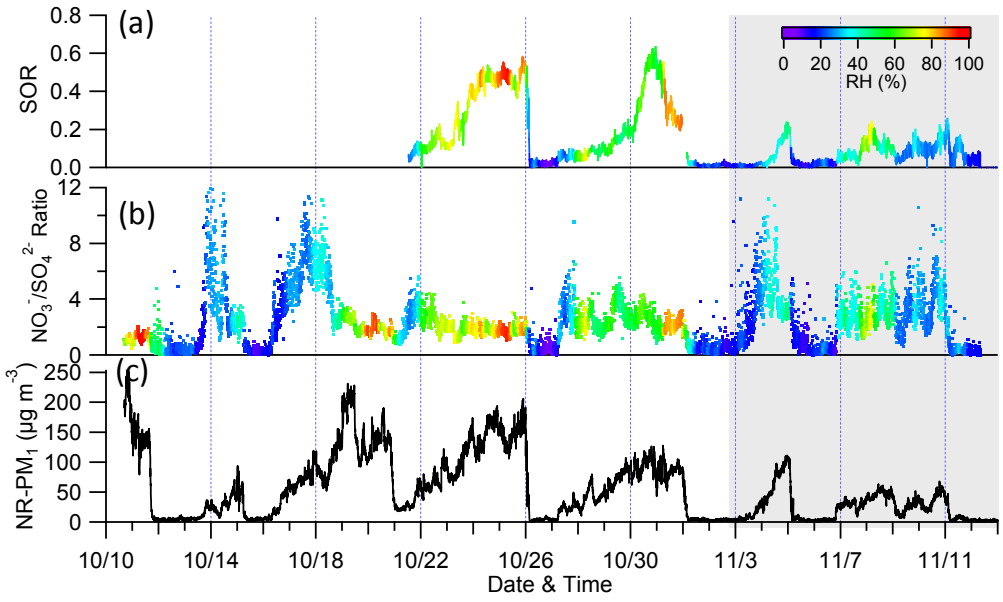

982

983 **Figure 3.** Time series of (a) sulfur oxidation ratio (SOR), (b) the ratio of NO_3^-/SO_4^{2-},
984 and (c) non-refractory submicron aerosol ($NR\text{-}PM_1$). The SOR and NO_3^-/SO_4^{2-} are
985 color coded by relative humidity (RH).

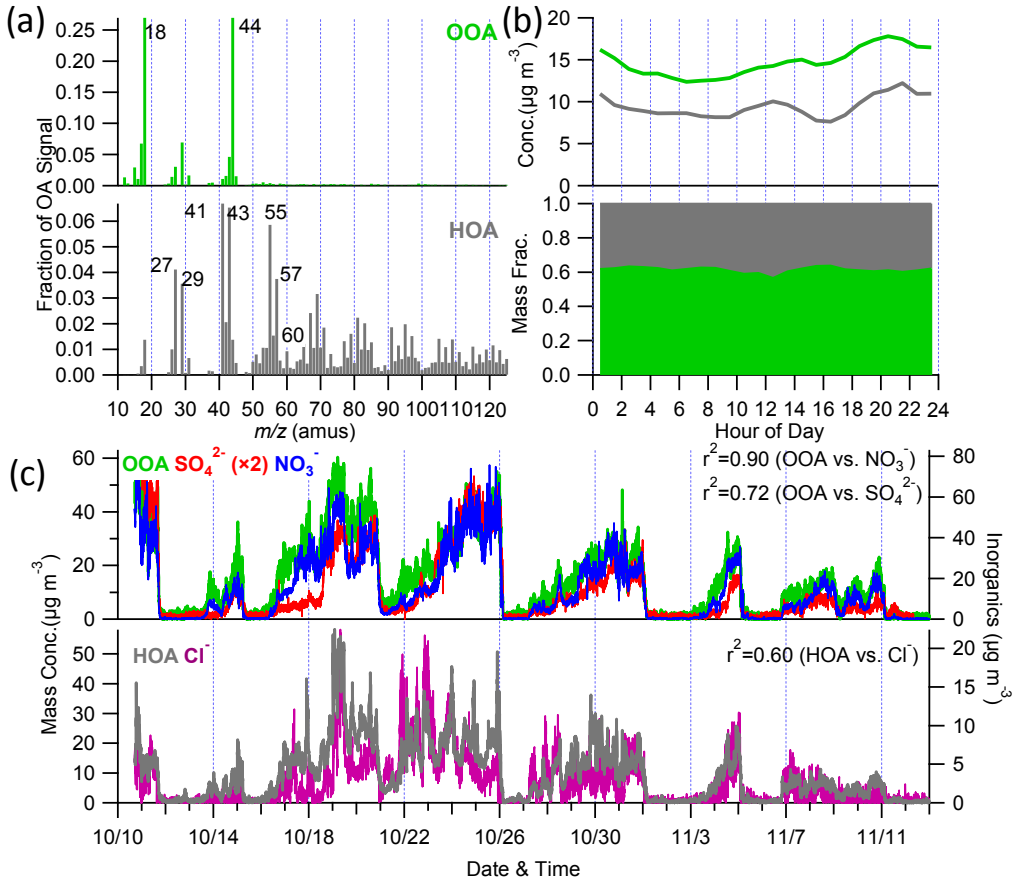

Figure 4. (a) Mass spectra of hydrocarbon-like organic aerosol (HOA) and oxygenated organic aerosol (OOA); (b) diurnal variations of the mass concentration and mass fraction of HOA and OOA; and (c) time series of HOA, OOA, and inorganic species (SO_4^{2-}, NO_3^-, Cl^-). The correlations of HOA and OOA with inorganic species are also shown in the figure.

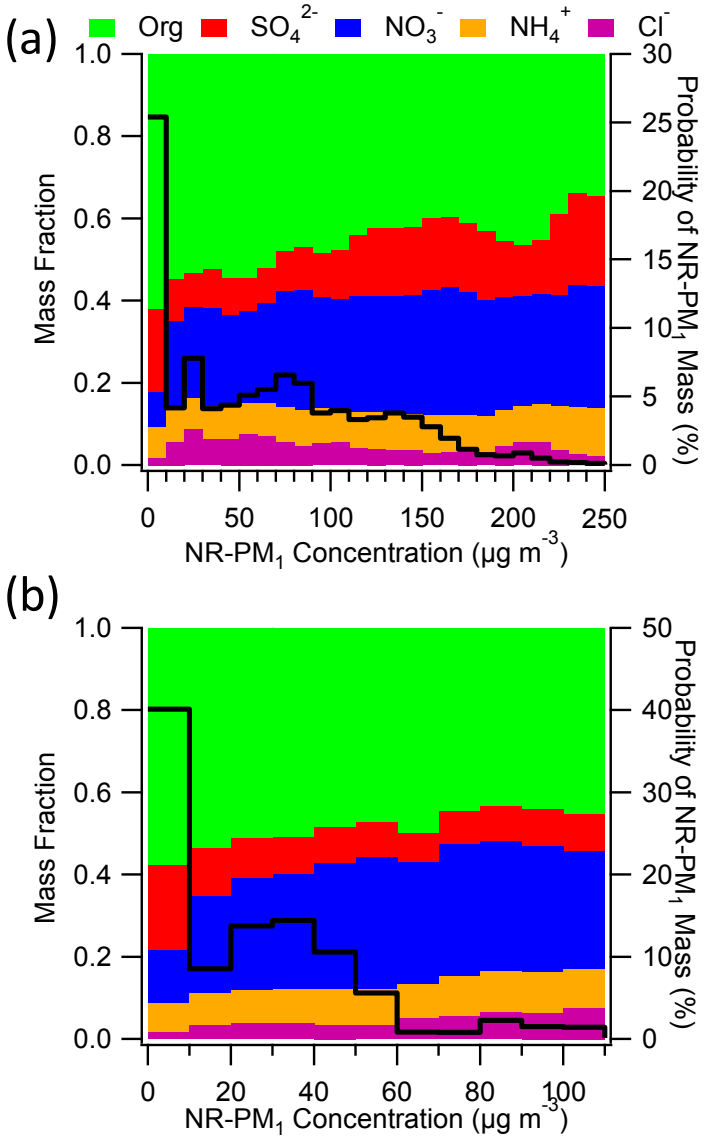

992

993 **Figure 5.** Submicron aerosol composition as a function of non-refractory submicron
994 aerosol ($NR\text{-}PM_1$) mass loadings (a) before the Asia–Pacific Economic Cooperation
995 (APEC) summit and (b) during APEC. The solid line shows the probability of the
996 $NR\text{-}PM_1$ mass.

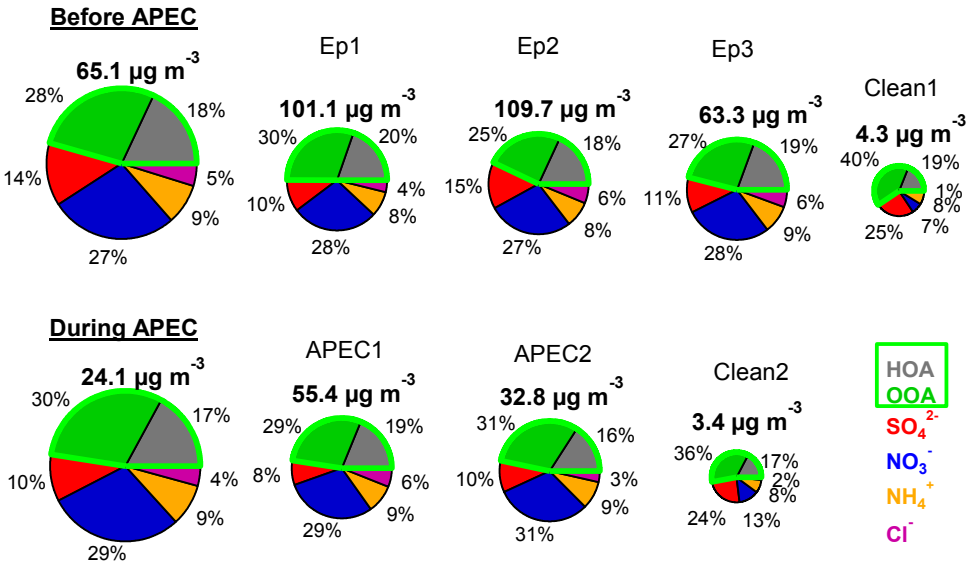

997

998 **Figure 6.** Average chemical composition of non-refractory submicron aerosol
999 ($NR\text{-}PM_1$) before and during the Asia–Pacific Economic Cooperation (APEC) summit
1000 and that of five haze episodes and two clean events marked in Fig. 2.

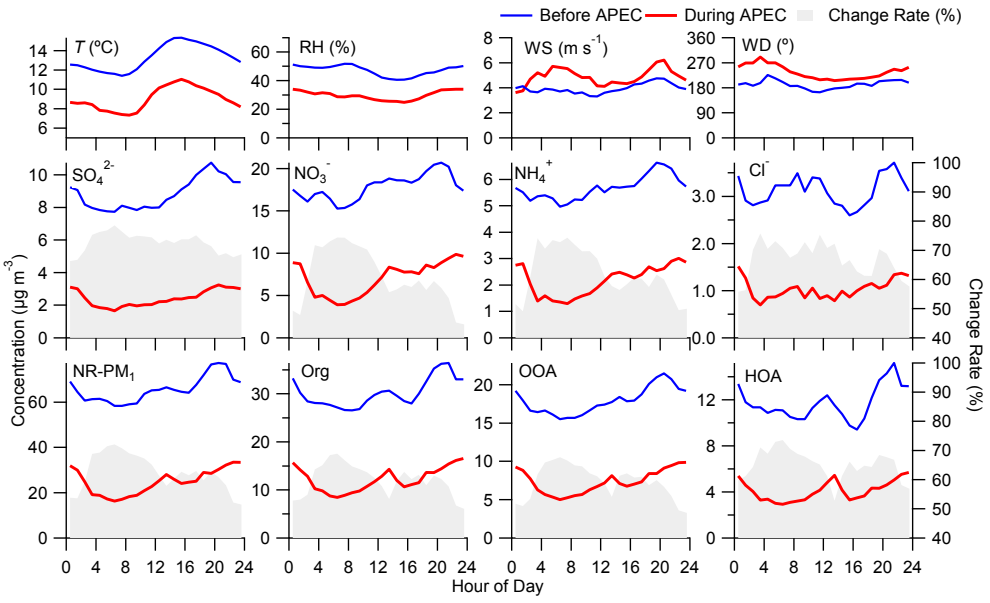

1001

1002 **Figure 7.** Diurnal variations of meteorological variables such as temperature (*T*),
1003 relative humidity (RH), wind speed (WS), and wind direction (WD); non-refractory
1004 submicron aerosol ($NR\text{-}PM_1$) species; and organic aerosol (OA) factors before and
1005 during the Asia–Pacific Economic Cooperation (APEC) summit. The change rates
1006 during APEC (= (Before APEC–APEC)/Before APEC × 100) are also marked in light
1007 gray in the figure.

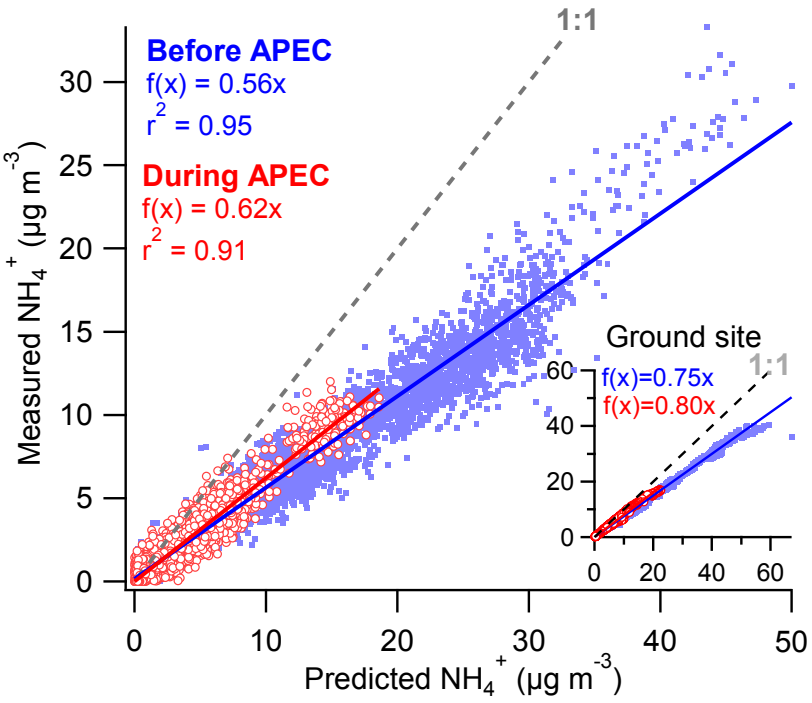

1008

1009 **Figure 8.** Correlations between measured NH_4^+ and predicted NH_4^+ (= 18 × (2 ×
1010 $SO_4^{2-}/96 + NO_3^-/62 + Cl^-/35.5$)) before and during the Asia–Pacific Economic
1011 Cooperation (APEC) summit. The inset plot shows the correlations of measured NH_4^+
1012 versus predicted NH_4^+ at the ground site.

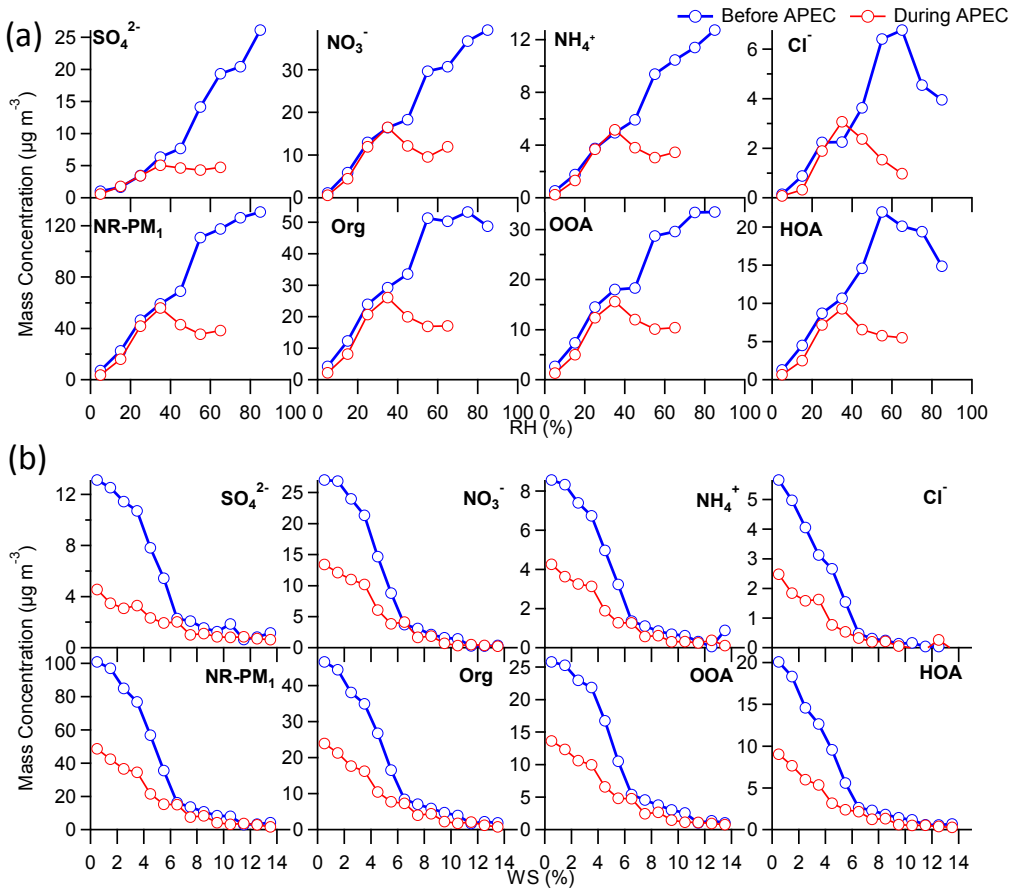

1013

1014 **Figure 9.** Variations of non-refractory submicron aerosol ($NR\text{-}PM_1$) species and
1015 organic aerosol (OA) factors as a function of (a) relative humidity (RH) and (b) wind
1016 speed (WS) before and during the Asia–Pacific Economic Cooperation (APEC)
1017 summit. The RH and WS were from the tower measurements at 280 m.

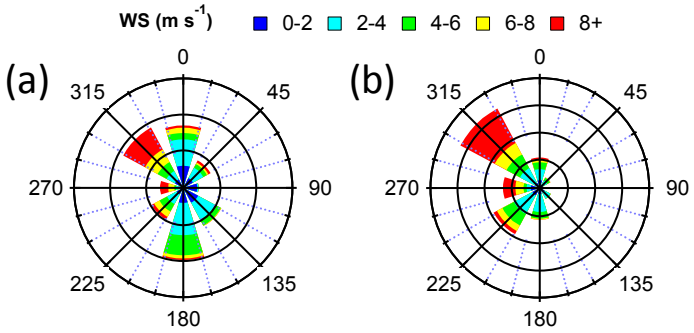

1018

1019 **Figure 10.** Wind increase plots (a) before the Asia–Pacific Economic Cooperation
1020 (APEC) summit and (b) during APEC.

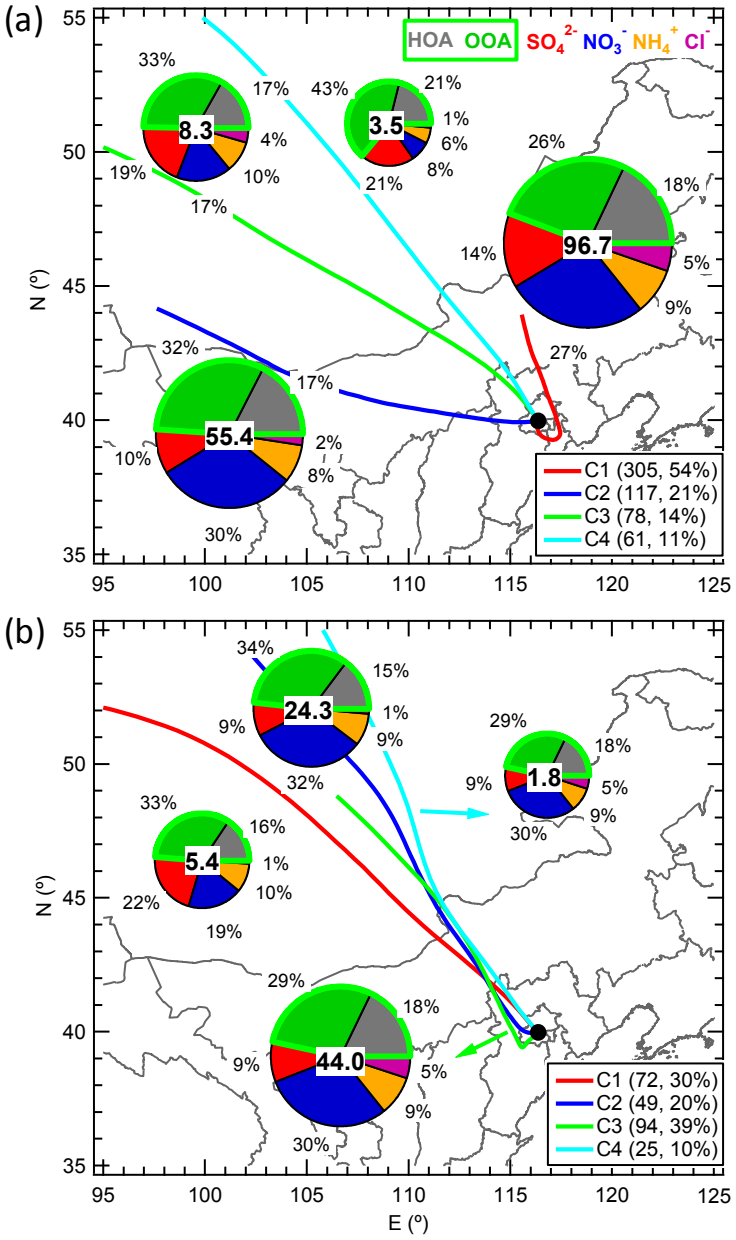

1021

1022 **Figure 11.** Average non-refractory submicron aerosol (NR-PM_1) composition for
1023 each cluster (a) before and (b) during the Asia–Pacific Economic Cooperation (APEC)
1024 summit. The numbers on the pie charts refer to the average total NR-PM_1 mass for
1025 each cluster. In addition, the number of trajectories and its percentage to the total
1026 trajectories are also shown in the legends.

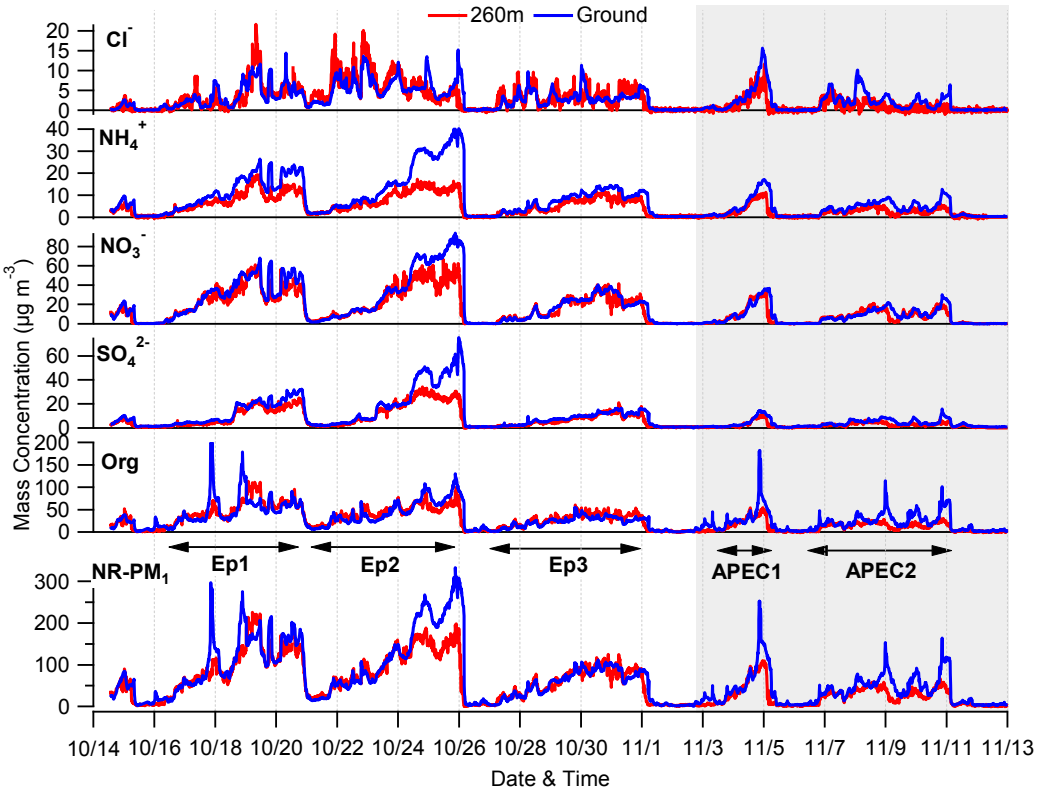

1027

1028 **Figure 12.** Comparisons of time series of total non-refractory submicron aerosol
1029 (NR-PM_1) mass and NR-PM_1 species between 260 m and the ground level.

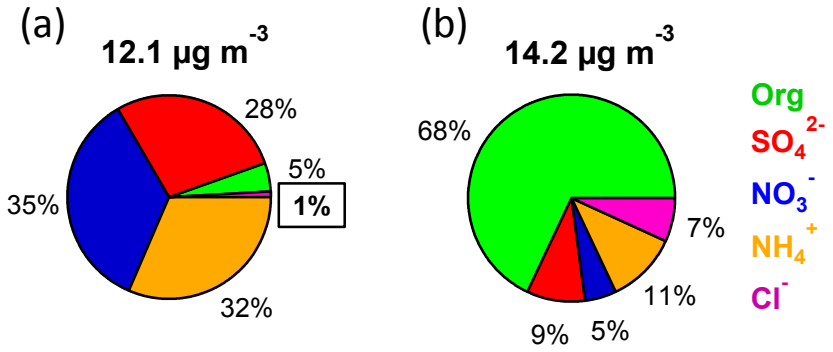

1030

1031 **Figure 13.** Average chemical composition of the difference between ground level and
1032 260 m (a) before the Asia–Pacific Economic Cooperation (APEC) summit and (b)
1033 during APEC. "1%" shown in the box indicates a lower concentration of chloride at
1034 the ground site than that at 260 m.

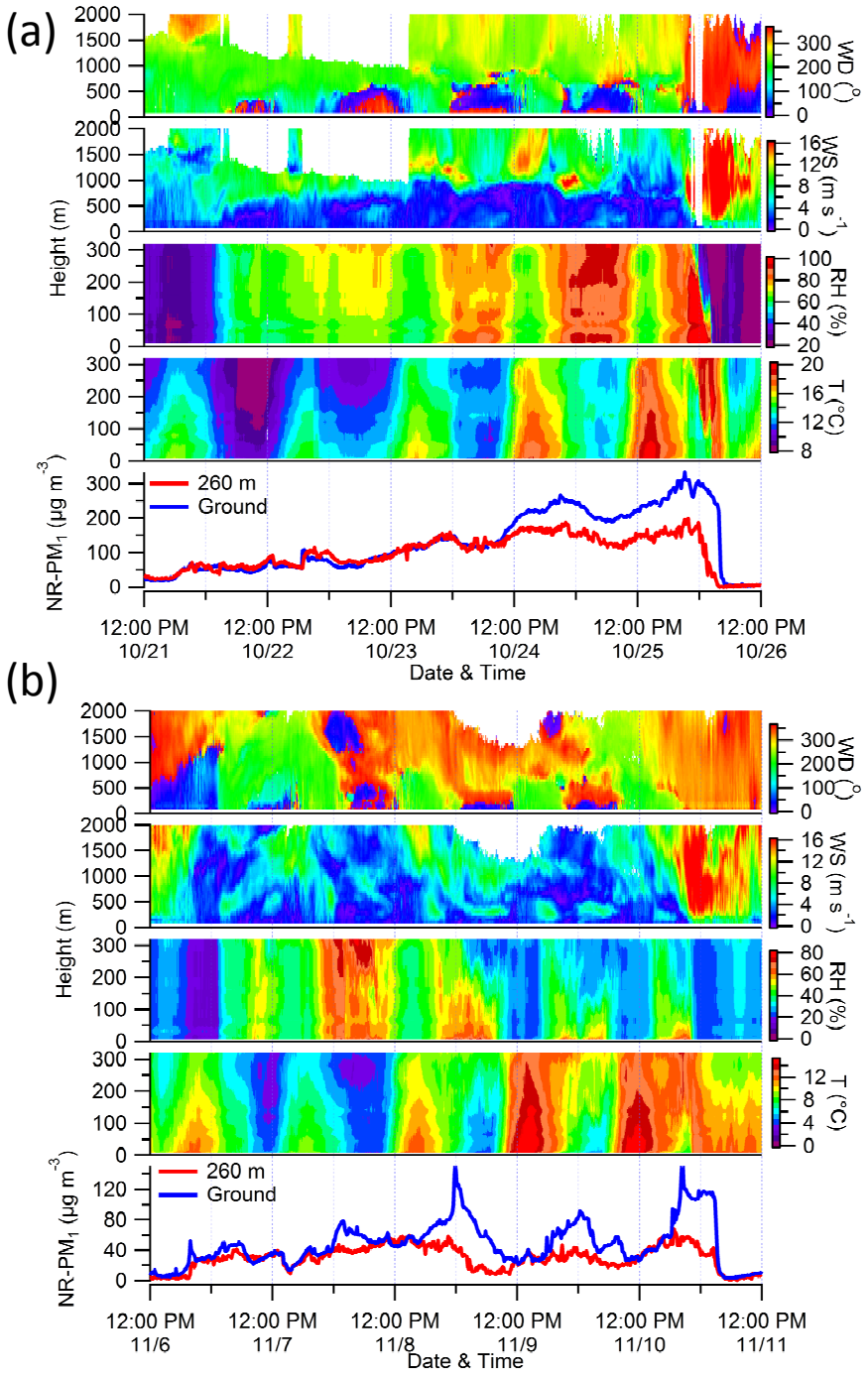

Figure 14. Evolution of vertical profiles of meteorological variables such as wind direction (WD), wind speed (WS), relative humidity (RH), and temperature (*T*) and non-refractory submicron aerosol ($NR\text{-}PM_1$) concentration at 260 m and the ground site during two pollution episodes (a) Ep2 and (b) APEC2. The vertical profiles of wind speed and wind direction were from the measurements of the Doppler wind lidar, and those of RH and T were from the tower measurements. The white areas in the figure indicate that the data were not available.